Molecular Models of Aging: Comparative Analysis of Gene Signatures in Replicative Senescence and Stress Induced Premature Senescence

A Thesis submitted in partial fulfillment of the requirements for the degree of Master of Science at George Mason University

by

Kamil Can Kural
Bachelor of Science
Montana State University, 2014

Director: Dr. Ancha Baranova, Associate Professor
School of Systems Biology

Fall Semester 2016
George Mason University
Fairfax, VA

DEDICATION

To my parents Hulya and Gunduz.

Thank you for your continued support. This work couldn't have been possible without your selfless devotion to my education.

To my aunt Fatos and her family

Thank you for opening your home to me in difficult times and standing behind me against all sorts of trouble. I will be forever in your debt.

To friends, family and colleagues who have contributed in work, thought and support to this project.

ACKNOWLEDGEMENTS

I would like to thank my advisor, Dr. Ancha Baranova, whose patience, guidance and support helped me throughout this study. This thesis wouldn't have been possible without her mentorship and ever ending support. It was a pleasure to work with her. She is very generous with her knowledge, wisdom and compassion. Thank you for believing in me and providing a world of opportunities.

I would like to thank Dr. Birerdinc for her devotion. She has been very helpful with her thoughts, knowledge and advice. She helped me tremendously in my journey of obtaining a Master's Degree with her ideas.

Thanks to Dr. Seto for his enlightening classes and brilliance. Without him, I wouldn't be in this program.

Thanks to all faculty members of School of Systems Biology and Bioinformatics Program. You make this university a warm and great place for learning with your efforts.

A very special thanks to my friends in Turkey and around the world for their continuing moral support and lighting my spirit up in bad times. I sincerely wish that you get the life you deserve after overcoming the hardships we have all been facing.

TABLE OF CONTENTS

LIST OF TABLES

LIST OF FIGURES

LIST OF ABBREVIATIONS

Replicative Senescence ..... RS
Stress-Induced Premature Senescence ..... SIPS
E3 Ubiquitin-Protein Ligase Mdm2 ..... MDM2
Stromelysin MMP3
Alpha-1,3-Mannosyl-Glycoprotein 2-Beta-N-Acetylglucosaminyltransferase MGAT1
H6 Family Homeobox 1 ..... HMX1
Iroquois Homeobox 2 ..... IRX2
Highly Divergent Homeobox ..... HDX
Homeobox C13 ..... HOXC13
Osteopontin SPP1
Deoxyribonucleic Acid ..... DNA
Ultraviolet ..... UV
Differentially Expressed Genes ..... DEGs
Gene Expression Omnibus ..... GEO
National Center for Biotechnology Information ..... NCBI
Robust Multi-Array Average ..... RMA
Gene Ontology ..... GO
Position Weight Matrices ..... PWMs
Transcription Start Site ..... TSS
Transcription Factor Binding Site ..... TFBS
False Discovery Rate ..... FDR
Maryland ..... MD
4-Aminobutyrate Aminotransferase ..... ABAT
Glutamate-Cysteine Ligase Modifier Subunit ..... GCLM
Glutaminase ..... GLS
Purine Nucleoside Phosphorylase ..... PNP
5'-Nucleotidase Ecto NT5E
Nicotinamide Phosphoribosyltransferase ..... NAMPT
Nicotinamide Nucleotide Adenylyltransferase 2 ..... NMNAT2
Adenosine Monophosphate Deaminase 3 ..... AMPD3
Activator of basal transcription ..... ABT
Ornithine decarboxylase ODC1
Ethanolaminephosphotransferase 1 ..... EPT1
1-phosphatidylinositol 4,5-bisphosphate phosphodiesterase beta-4 ..... PLCB4
Homeobox B13 ..... HOXB13
MYC Associated Zinc Finger Protein ..... MAZ

Krueppel-like factor 4 ..... GKLF
GLI Family Zinc Finger ..... GLI
IK Cytokine, Down-Regulator of HLA II ..... IK
Specificity Protein 1 Transcription Factor SP1
Zinc Finger and BTB Domain Containing 16 ..... PLZF
Pre-B-Cell Leukemia Transcription Factor ..... PBX
Mono-unsaturated Fatty Acid ..... MUFA
Poly-unsaturated Fatty Acid ..... PUFA
Caudal Type Homeobox 2 ..... CDX2
X-linked cleft palate (CPX) disorder gene ..... CPXH
POU Class 4 Homeobox 1 ..... POU4F1
Immortalized Human Keratinocyte cell line ..... HaCaT
Quantitative Real-Time Polymerase Chain Reaction ..... qRT-PCR
AKT Serine/Threonine Kinase 1 ..... AKT1
Vascular Endothelial Growth Factor A ..... VEGFA
Insulin ..... INS

ABSTRACT

MOLECULAR MODELS OF AGING: COMPARATIVE ANALYSIS OF GENE SIGNATURES IN REPLICATIVE SENESCENCE AND STRESS INDUCED PREMATURE SENESCENCE

Kamil Can Kural, M.S.

George Mason University, 2016

Thesis Director: Dr. Ancha Baranova

In culturing normal diploid cells, senescence may either happen naturally, in the form of replicative senescence, or it may be a consequence of external challenges such as oxidative stress. In this work, a comparative analysis design has been used that aims to reconstruct the molecular cascades which are specific for replicative senescence (RS) and stress-induced senescence (SIPS) in human fibroblasts. The results indicate the involvement of caspase-3/keratin-18 pathway and serine/threonine kinase Aurora A/ MDM2 pathway commonly shared between RS and SIPS. Moreover, stromelysin/MMP3 and N-acetyl glucosaminyl transferase enzyme MGAT1, which initiates the synthesis of hybrid and complex N-glycans, were identified as key orchestrating components in RS and SIPS, respectively. In RS only, Aurora-B driven cell cycle signaling was deregulated in concert with the suppression of anabolic branches of the fatty acids and estrogen metabolism. In SIPS, Aurora-B signaling is deprioritized, and the synthetic branches of

cholesterol metabolism are upregulated, rather than downregulated, while proteasome/ubiquitin ligase pathways of protein degradation dominate the regulatory landscape. This picture indicates that SIPS proceeds in cells that are actively fighting stress which facilitates premature senescence while failing to completely activate the orderly program of RS. The promoters of genes differentially expressed in either RS or SIPS are unusually enriched by the binding sites for Homeobox family proteins, with particular emphasis on HMX1, IRX2, HDX and HOXC13. Additionally, Iroquois Homeobox 2 (IRX2) was identified as a master regulator for the secretion of SPP1-encoded Osteopontin, a stromal driver for tumor growth that is overexpressed by both RS and SIPS fibroblasts. The latter supports the hypothesis that senescence-specific de-repression of SPP1 aids in SIPS-dependent stromal activation.

1. INTRODUCTION

An Overall Summary for the Thesis

All biological organisms share a universal feature called aging. In multicellular organisms, the major consequence of aging is a functional deficiency of cells, tissues and organs. Additionally, renewable cells and tissues display deficits in regenerative capacities that are paralleled by an increase in incidence of hyperplasia, a gain-of-functional change that allow cells to proliferate inappropriately [1]. The most serious type of hyperplasia is known as cancer.

In order to understand the aging process, model experiments are of crucial importance. Majority of well-known cellular models were developed at the time of the boom in cell and tissue culturing, providing a trove of important insights into cellular physiology. In particular, one of the pioneers in cell culture, Leonard Hayflick, showed that normal, non-transformed cells in culture can go through a limited number of divisions upon reaching the end of their replicative life span [2]. This finite number of divisions has been termed as the Hayflick limit.

Over the decades, it was discovered that proliferating cells reach the Hayflick limit largely because repeated DNA replication in the absence of telomerase causes telomeres

to shorten and eventually affect chromosomal stability and genome functioning [3]. The cells undergoing replicative senescence (RS) became enlarged in size and demonstrate systemic changes in expression level of many genes. The entry into the senescent state is mediated by at least two distinct signaling cascades linked to the activation of two tumor suppressing proteins, the p53/ p21 and p16INK4a/pRB pathways [4]. On the other side, cells exposed to various concentrations of different DNA damaging agents such as bleomycin, tert-butylhydroperoxide, hydrogen peroxide or doses of UV A and UV B also become post-mitotic and display signs of senescence. Latter phenomenon is termed as stress induced premature senescence (SIPS) [5]. The expression levels of many genes are changed during SIPS. It is believed that cellular and molecular mechanisms promoting an entry into senescence also provide protection against tumor formation [6, 7]. Identification and understanding the differences between RS and SIPS senescence is critical for the development of anti-aging strategies that do not induce tumorigenesis.

The main purpose behind this study was to identify the differentially expressed genes (DEGs) that distinguish the processes of replicative and stress induced senescence and to reconstruct relevant molecular cascades. To achieve this goal, a bioinformatics software platform called GeneXplain was employed that allowed both upstream and downstream analysis of DEGs validated by three-way comparisons of each type of senescent cells against the young cells (control group) and against each other. In both types of senescence, master regulators of genes were identified. Iroquois Homeobox 2 (IRX2) was also identified as the master regulator for the expression of SPP1-encoded osteopontin, a

secreted stromal driver for tumor growth that is overexpressed by both RS and SIPS fibroblasts.

Taking a Bioinformatics Perspective to Aging.

Aging is an unquestionably complex process. It is evident that even in cases like single point mutations and environmental stress, the effects on the aging process are neutralized via coordinated responses on a very large number of proximate mechanisms, most of which control integrity of the organism's network of self-repair and reproductive functions. The most important feature of lifespan modifying aspects of an organism is that they act on the average length of life without substantially interfering with the inherent process of senescence that causes disease, disability and defects. There are also many questions regarding to the variable rate of aging process even though genetic and environmental conditions are made as uniform as possible.

The obvious complexity of ageing is in fact comes from a direct prediction of the evolutionary understanding of aging, which originates from the disposable soma theory, combining within a single framework that answers to the questions of why and how ageing occurs [8]. While living, organisms face with many environmental stress that results with formation of defects at all levels of structure and function. This leaning of defects towards increased accumulation is countered by the control of an extensive array

of error-preventing and error-correcting mechanisms. However, repair and maintenance comes with an increased cost with time.

While it is not yet certain what mechanisms drive aging, it is evident that genes play a role. Several hundred genes have been identified that either speed up or slow aging if manipulated in model organisms until today [9]. An example is the gene *daf-2*, which encodes an insulin-receptor homologue in the nematode worm Caenorhabditis elegans. Gene activity stamps provide the optimal bar code to characterize the kind and status of a living system. These signatures can be used as they are, just as a marker for a certain phenomenon of interest, e.g., as biomarker of a specific disease or complex events like aging. Since gene activity is only a layer of information that needs to be combined with other layers of information to get a better understanding of aging process, scientists need to approach this with a new perspective. In order to look at the whole picture, an integrative path that can effectively combine the respective strengths of the reductionist and integrative strategies is needed. A smarter way to link everything would be to investigate intracellular mechanisms that underlie age-related damage, understand how the accumulated damage in cells, which may vary considerably between one individual cell and its neighbors, gives rise to age-related declines in tissue function and how these lower level changes both affect the viability of the organism as a whole as well as how systemic factors, such as hormones, provide scope for integration across multiple levels [10]. The necessary integration to convey this teamed-up understanding of aging is

possible by the multi-disciplinary framework of Bioinformatics and Computational Biology.

A widely used conventional method is done by finding differentially expressed genes and mapping them to ontologies. However, they provide very little insight into the pathways, interactions and causes of differential gene expression.

Upstream Analysis [11] on the other hand, which was employed into Genexplain bioinformatics platform, is a state-of-the-art analysis method for the promoter structures of the identified DEGs, infers the involved transcription factors (TFs), and identifies the signaling pathways that activate these TFs. In a final step, convergence points of these pathways are identified as potential master regulators or key nodes. By choosing this method, it is possible to obtain insights into promoters, their binding sites, transcription factor regulations, differential gene expression and master molecules responsible of aging effects. Combining all of these together provides a better causality of the observed changes in a given system, which might not have been achieved before this study.

2. MATERIALS AND METHODS

2.1 Microarray Data and Differential Gene Expression Analysis

To investigate both types of senescence, publicly available dataset GSE13330 was downloaded from Gene Expression Omnibus (NCBI, Bethesda, MD, USA). This dataset is comprised of 16 samples profiled using Affymetrix Human Genome U133 Plus 2.0 Array. In this dataset, replicative-senescent human foreskin BJ fibroblasts and young fibroblast controls were assayed in 6 biological replicates each. An induction of cell senescence by stress was performed with 100ug/ml of bleomycin sulfate, and analyzed in four biological replicates [12].

Raw data of stress induced and replicative senescence, as well as data on younger control cells were normalized and background corrected using RMA (Robust Multi-Array Average). The Limma (Linear Models for Microarray Data) method [13, 14] was applied to define fold changes of genes and to calculate adjusted p-values using a Benjamini-Hochberg adjusted p-value cutoff (.05). The up-regulated genes were filtered using the filter: logFC>0.5 && adj_P_Val<0.05. Down-regulated genes were filtered using the filter: logFC<-0.5 && adj_P_Val<0.05.

2.2 Functional Enrichment Analysis

DEGs were analyzed using the GeneXplain bioinformatics software platform (http://www.genexplain.com/). Using the workflows in geneXplain framework, the sets of up and down regulated genes for both SIPS and RS were mapped to various gene ontologies, i.e. biological processes, cellular components, molecular functions, reactome pathways, TRANSPATH® [15] pathways and transcription factor classification.

The output links each gene to GO identifiers that are, in turn, are hyperlinked to the page http://www.ebi.ac.uk/QuickGO/ with information about this ontological term. Ontological classification evaluates statistical significance for each term; the resultant p-values were used for further interpretation of the results.

2.3 Promoter Analysis

The sets of up- and down-regulated genes identified in each comparison were subjected to the promoter analysis using TRANSFAC [16] database of position weight matrices (PWMs) characteristic for vertebrate genomes (vertebrate_non_redundant_minSUM database subdivision). Each promoter was defined as the sequence within -1000 to +100 coordinates, where the TSS of the main transcript of each gene was the point 0.

The TFBS search on promoter sequences was done using the MATCH algorithm [17, 18] integrated into the GeneXplain platform and executed within the pre-defined workflows.

The promoter sequences and annotations of TSS positions were according to the Ensembl database (version hg19 build 72.37).

2.4 Identification of Master Regulators

Lists of DEGs upregulated in each of cell senescence types were used as inputs in a search for master regulatory key molecules that influence the senescence pathways [17]. The search was performed in the TRANSPATH® database networks with a maximum radius of 10 steps upstream of an input gene set, a default cut-off scores at 0.2, and for FDR at 0.05 and Z-score at 1.0.

2.5 Pathway Studio - Guided Analysis of Osteopontin Regulation

To construct a concise network that bridges senescence regulators highlighted by GeneXplain–guided analysis of DEGs, we used the Pathway Studio software (Elsevier, Rockville, MD) that is able to dynamically create and draw protein interaction networks and pathways. Each node represents either a molecular entity or a control mechanism of the interaction. In this study, the shortest path analysis function was utilized predominantly.

3. RESULTS

Extraction of gene signatures important in replicative and stress-induced cell senescence was performed using public 16-sample dataset GSE13330 previously described in [12]. We divided the study into two parts. First, the signaling events that are shared in both RS and SIPS were analyzed. Secondly, DEGs and respective signaling events uniquely describing each type of senescence were identified.

To dissect the differences between RS and SIPS, 1) six biological replicates of replicative senescent fibroblasts were compared to six biological replicates of young fibroblasts and yielded 1994 downregulated and 2818 upregulated mRNAs; 2) four biological replicates of bleomycin induced senescent fibroblasts were compared to six replicates of young fibroblast cultures (3082 downregulated and 2768 upregulated mRNAs); 3) six biological replicates of replicative senescent fibroblasts were compared to four biological replicates of bleomycin induced senescent fibroblasts (2724 downregulated and 1628 upregulated mRNAs). Each list of DEGs was divided into up- and downregulated sections. A comparison of the three DEG lists that resulted from comparisons described above has identified 524 shared between RS and SIPS (Fig.1 and 2 for downregulated (N=282) and upregulated (N=242) genes, respectively). All these mRNAs exhibited a change in expression levels of more than two fold in all three types of the profiled cells.

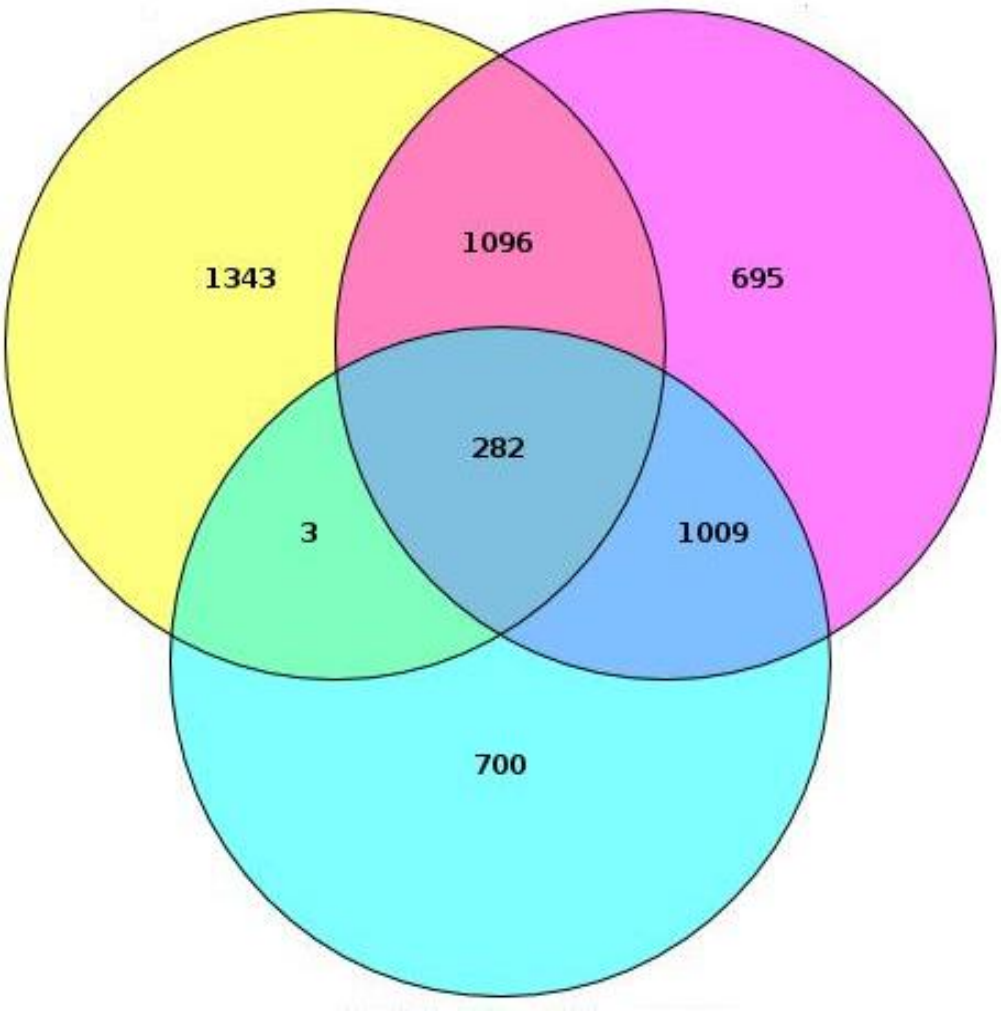

Figure 1: Venn Diagram for lists of Downregulated Genes

Venn diagram for lists of downregulated genes common and specific for each type of cell senescence. Yellow circle represents the comparison of Bleomycin Treated cells to Replicative Senescent cells. Purple circle represents the comparison of Bleomycin Treated cells to Young Controls. Blue circle represents the comparison of Replicative Senescent cells and Young Controls.

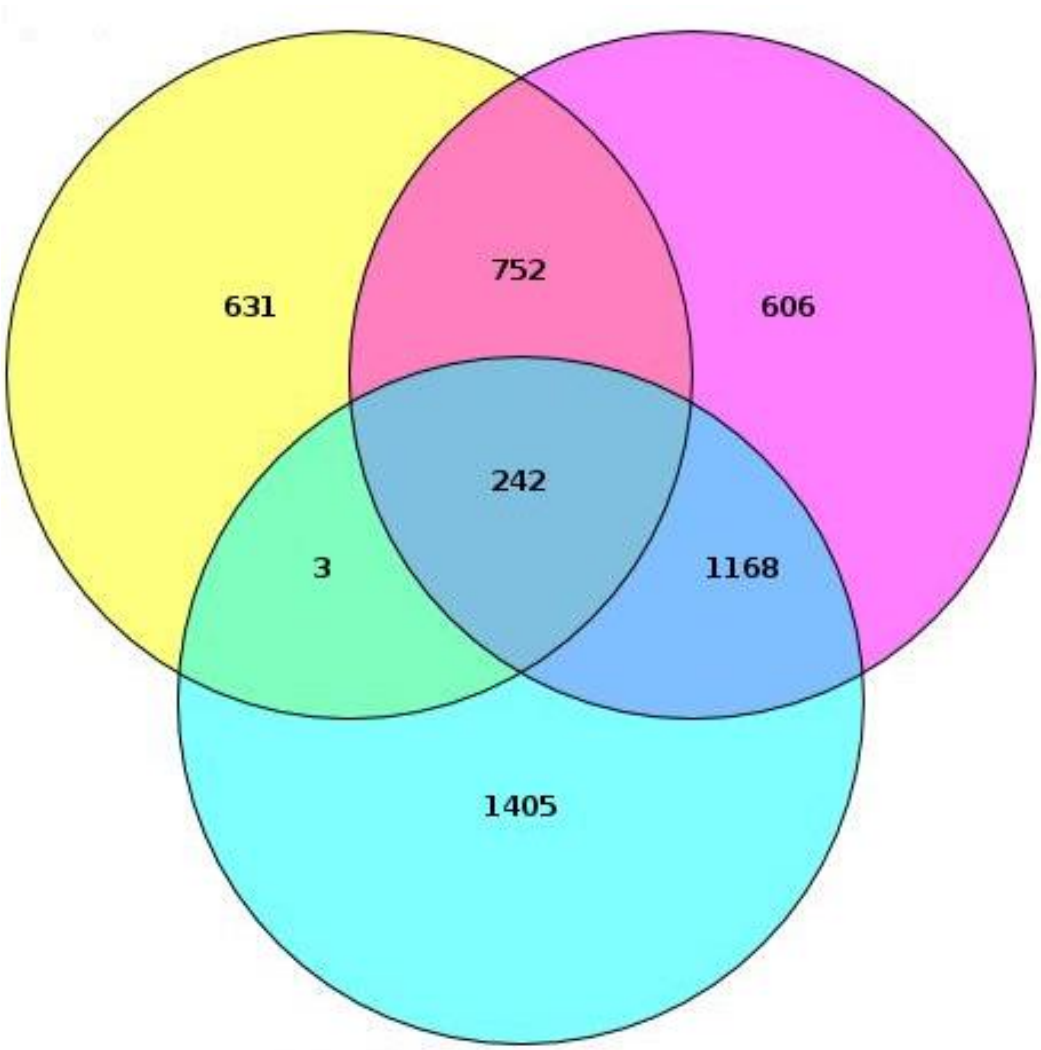

Figure 2: Venn Diagram for Lists of Upregulated Genes

Venn diagram for lists of upregulated genes common and specific for each type of cell senescence. Yellow circle represents the comparison of Bleomycin Treated cells to Replicative Senescent cells. Purple circle represents the comparison of Bleomycin Treated cells to Young Controls. Blue circle represents the comparison of Replicative Senescent cells and Young Controls.

3.1 Genes Responsible of Bleomycin Induced and Replicative Senescence

A total of 1410 genes were upregulated and a total of 1291 genes were downregulated both in RS and SIPS as compared to younger control fibroblasts. Resultant lists of up- and downregulated genes were subjected to functional analysis separately. Each gene was mapped to GO biological processes, GO cellular components, GO molecular functions, Reactome, HumanCyc, TF classification and the latest TRANSPATH® [15] available in the GeneXplain platform.

Caspase-3/keratin-18 and Aurora A kinase/MDM2 pathways were the most upregulated signaling events commonly dominating regulatory landscapes in both bleomycin-induced and replicative type of senescence (adjusted P-values < 0.009 for each of these signaling events). Concerted upregulation of many enzymes participating in glutamate (ABAT, GCLM, GLS), nucleotide (PNP, NT5E, NAMPT, NMNAT2, AMPD3), polyamine (ABT, ODC1) and choline (EPT1, PLCB4) metabolic branches was also noted (adjusted p-value range of <0.016 to < 0.05 for various fragments of these metabolic cascades) (Table 1).

Table 1: Pathway Fragment Analysis

Pathway Fragment Analysis						
Pathway fragments down-regulated in both RS and SIPS						
Title	**Number of hits**	**Group size**	**Expected hits**	**P-value**	**Adjusted P-value**	**Hit names**
Glu ---GluR1:GluR3---> c-fos	2	11	0.11067	0.00504	0.02521	GRIA1 (ENSG00000155511), GRIA1 (ENSG00000269977)
GluR1:GluR2 complex	2	9	0.09055	0.00334	0.02521	GRIA1 (ENSG00000155511), GRIA1 (ENSG00000269977)
AMPA receptor signaling	2	14	0.14086	0.00819	0.0273	GRIA1 (ENSG00000155511), GRIA1 (ENSG00000269977)

wnt ---> beta-catenin	2	25	0.25153	0.02525	0.04864	TCF7L2, WNT2
SDF-1 ---> G-protein	2	27	0.27165	0.02918	0.04864	CXCL12, GNG2
SDF-1 ---> calcium mobilization	2	26	0.26159	0.02718	0.04864	CXCL12, GNG2
Pathway fragments up-regulated in both RS and SIPS						
Caspase-3 ---/ K18	2	3	0.04856	7.5719E-4	0.00909	CASP3, KRT18
Aurora-A(h) ---/ p53(h)	2	3	0.04856	7.5719E-4	0.00909	AURKA, MDM2
glutamate metabolism	3	16	0.25897	0.00189	0.01513	ABAT, GCLM, GLS
L-glutamate --- ammonia---> 2-oxoglutarate	2	8	0.12948	0.00671	0.01611	ABAT, GLS
xanthosine-5-phosphate ---> allantoin	2	8	0.12948	0.00671	0.01611	NT5E, PNP
IMP ---> xanthine	2	8	0.12948	0.00671	0.01611	NT5E, PNP
dGDP ---> guanine	2	7	0.1133	0.00509	0.01611	NT5E, PNP
dADP ---> hypoxanthine	2	7	0.1133	0.00509	0.01611	NT5E, PNP
L-ornithine ---> succinate	2	8	0.12948	0.00671	0.01611	ABAT, ODC1
polyamine metabolism	2	8	0.12948	0.00671	0.01611	ABAT, ODC1
plasmenylethanolamine ---> plasmenylcholine	2	10	0.16185	0.01057	0.02307	EPT1, PLCB4
GDP ---> xanthine	2	12	0.19423	0.01519	0.03039	NT5E, PNP
interconversions and degradations of purine ribonucleotides	3	41	0.6636	0.02728	0.04365	AMPD3, NT5E, PNP

L-tryptophan ---> NAD+, NADPH	2	16	0.25897	0.02653	0.04365	NAMPT, NMNAT2
biosynthesis and degradation of nicotinamide,NAD+,NADP+	2	16	0.25897	0.02653	0.04365	NAMPT, NMNAT2
plasmenylcholine biosynthesis	2	19	0.30752	0.03667	0.05501	EPT1, PLCB4
Pathway fragments down-regulated in RS						
acetyl-CoA, acetoacetyl-CoA ---> cholesterol, fatty acid	7	21	0.90945	1.6325E-5	5.7683E-4	FDFT1, FDPS, HMGCS1, IDI1, LSS, MVD, SQLE
cholesterol metabolism	7	21	0.90945	1.6325E-5	5.7683E-4	FDFT1, FDPS, HMGCS1, IDI1, LSS, MVD, SQLE
biosynthesis of saturated and n - 9 series of MUFA and PUFA	5	9	0.38976	1.5131E-5	5.7683E-4	ELOVL6, FADS1, FADS2, FASN, SCD
17-alpha-hydroxyprogesterone ---> 5alpha-androstanediol	3	5	0.21654	7.3989E-4	0.01569	AKR1C1 (ENSG00000187134), AKR1C2 (ENSG00000151632), SRD5A3

acetyl-CoA, malonyl-CoA ---> lignoceric acid	3	5	0.21654	7.3989E-4	0.01569	ELOVL6, FADS2, FASN
HMGCR regulation	9	65	2.81496	0.00158	0.02785	EGFR, FDFT1, FDPS, HMGCS1, IDI1, INSIG1, LSS, MVD, SQLE
Pathway fragments up-regulated in RS						
Aurora-B cell cycle regulation	17	55	4.09011	1.676E-7	4.0727E-5	BIRC5, BUB1, BUB1B, CCNB1, CCNB2, CDC20, CDCA8, CDK1, CENPE, CUL1, INCENP, MAD2L1, PLK1, TTK, UBB, UBE2C, ZC3HC1

Cdk1, Plk1 ---/ cyclin B	5	5	0.37183	2.1527E-6	1.7437E-4	CCNB1, CDC20, CDK1, CKS1B, PLK1
Plk1 ---> Bub1	5	5	0.37183	2.1527E-6	1.7437E-4	BUB1, CCNB1, CCNB2, CDK1, PLK1
Plk1 ---> INCENP	5	6	0.44619	1.2138E-5	7.3737E-4	CCNB1, CCNB2, CDK1, INCENP, PLK1
Plk1 activation and substrates	9	24	1.78478	2.7847E-5	0.00135	BRCA2, CCNB1, CCNB2, CDK1, KIF23, PLK1, PRKACB, RAD51, STK10
CENP-E ---> BubR1	5	7	0.52056	3.9925E-5	0.00162	BUB1, BUB1B, CENPE, MAD2L1, TTK
cyclosome regulation	16	75	5.57743	7.6369E-5	0.00265	CCNA2, CCNB1,

						CCNB2, CDC20, CDK1, CKS1B, CUL1, FBXO5, MAD2L1, NDC80, PLK1, SKP2, UBB, UBE2C, UBE2E2, UBE2S
cyclosome regulatory network	16	77	5.72616	1.0692E-4	0.00289	CCNA2, CCNB1, CCNB2, CDC20, CDK1, CKS1B, CUL1, FBXO5, MAD2L1, NDC80, PLK1, SKP2, UBB, UBE2C, UBE2E2, UBE2S
Cdc20 ubiquitination	8	22	1.63605	1.03E-4	0.00289	BUB1B, CCNB1, CDC20,

						CDK1, CKS1B, MAD2L1, UBB, UBE2C
Cdc20 deubiquitination	8	23	1.71041	1.4802E-4	0.0036	BUB1B, CCNB1, CDC20, CDK1, CKS1B, MAD2L1, UBB, UBE2C
Plk1 cell cycle regulation	12	52	3.86702	2.8909E-4	0.00585	BRCA2, CCNB1, CCNB2, CDK1, CUL1, FBXO5, KIF23, PLK1, PRKACB, RAD51, STK10, UBB
Metaphase to Anaphase transition	12	52	3.86702	2.8909E-4	0.00585	BUB1, BUB1B, CCNB1, CDC20, CDK1, CKS1B,

						FBXO5, MAD2L1, NEK2, PLK1, UBB, UBE2C
Bub1 ---> APC7	4	6	0.44619	3.9379E-4	0.00736	BUB1, BUB1B, CDC20, MAD2L1
S phase (Cdk2)	12	55	4.09011	5.0416E-4	0.00875	CCNA2, CDK1, CDKN3, CKS1B, CUL1, E2F3, E2F8, PPM1A, PPM1B, PPM1D, SKP2, UBB
ID complex deubiquitylation	4	7	0.52056	8.6562E-4	0.01402	CDK1, FANCD2, FANCI, UBB
borealin ---> Aurora-B	3	4	0.29746	0.00153	0.02323	BIRC5, CDCA8, INCENP
Pin1 ---> APP	3	5	0.37183	0.00361	0.05167	CCNB1, CCNB2, CDK1

Pathway fragments down-regulated in SIPS						
NO SIGNIFICANT FINDINGS						
Pathway fragments up-regulated in SIPS						
HMGCR regulation	21	65	6.1986	1.9691E-7	6.4979E-5	CAB39, CAB39L, CYP51A1, DHCR7, EGFR, FDFT1, FDPS, HMGCS1, IDI1, LIPA, PSMA7, PSMC1, PSMC4, PSMC5, PSMD11, PSMD2, PSMD8, SC5D, TM7SF2, UFD1L, VCP
Acetyl-CoA, acetoacetyl-CoA ---> cholesterol, fatty acid	9	21	2.00262	5.8742E-5	0.00646	CYP51A1, DHCR7, FDFT1, FDPS, HMGCS1, IDI1, LIPA, SC5D, TM7SF2
cholesterol metabolism	9	21	2.00262	5.8742E-5	0.00646	CYP51A1, DHCR7, FDFT1, FDPS, HMGCS1, IDI1, LIPA, SC5D, TM7SF2
parkin associated pathways	15	65	6.1986	8.2044E-4	0.03437	CALM2, DNAJA1, HSPA8, PSMA7, PSMC1, PSMC4, PSMC5, PSMD11, PSMD2, PSMD8, TUBA1C, TUBB6, UBE2G1, UBE2L3, UBE2N

Mdm2 ---> p/CAF	8	23	2.19335	8.3317E-4	0.03437	PSMA7, PSMC1, PSMC4, PSMC5, PSMD11, PSMD2, PSMD8, TAF9 (ENSG00000085231)
HMGCR ---> 26S proteasome	9	28	2.67017	7.5931E-4	0.03437	PSMA7, PSMC1, PSMC4, PSMC5, PSMD11, PSMD2, PSMD8, UFD1L, VCP
ER-alpha ---CHIP---> 26S proteasome	9	28	2.67017	7.5931E-4	0.03437	HSP90AA1, HSPA8, PSMA7, PSMC1, PSMC4, PSMC5, PSMD11, PSMD2, PSMD8
cofilin-1 degradation	8	22	2.09799	5.9124E-4	0.03437	CFL1, PSMA7, PSMC1, PSMC4, PSMC5, PSMD11, PSMD2, PSMD8
Smac ---/ cIAP-2	8	24	2.28871	0.00115	0.03446	BIRC3, PSMA7, PSMC1, PSMC4, PSMC5, PSMD11, PSMD2, PSMD8
E1 ---/ alpha-synuclein	8	24	2.28871	0.00115	0.03446	PSMA7, PSMC1, PSMC4, PSMC5, PSMD11, PSMD2, PSMD8, UBE2L3
NIK degradation	8	24	2.28871	0.00115	0.03446	PSMA7, PSMC1, PSMC4, PSMC5,

						PSMD11, PSMD2, PSMD8, TRAF3
Caspase network	17	82	7.81977	0.00137	0.03759	BID, BIRC3, CDC42, CFLAR, CRADD, DFFA, HSPD1, MCL1, PSMA7, PSMC1, PSMC4, PSMC5, PSMD11, PSMD2, PSMD8, UBE2L3, XIAP

Among the most downregulated signaling events significantly overrepresented in both bleomycin-induced and replicative type of senescence were GluR/AMPA receptor (GRIA1 isoforms), wnt/beta-catenin (TCF7L2/WNT2) and SDF-1 cascades (adjusted p-value range of <0.026 to < 0.05 for various fragments of these signaling pathways).

Upstream analysis aimed at identifying potential transcription factor binding sites (TFBSs) overrepresented in the promoters of differentially expressed genes commonly deregulated in both types of senescence was performed after filtration of gene expression levels by log fold change (FC) of 1.5 for up-regulated (N=130 genes) and down-regulated (N=177) genes, separately. The algorithm for transcription factor binding site (TFBS) enrichment analysis has been described in Kel et al. [18].

The outputs shown in the tables (2, 3) include the matrices of the hits which are over-represented in the Yes track (study set) versus the No track (background set), with only the overrepresented matrices with Yes-No ratio higher than 1 included, and the highest Yes-No ratios reflecting higher degrees of matches enrichment for the respective matrix in the Yes set. Matrix cut-off value were calculated and associated with the P-value score of enrichment as described before [18, 19].

Table 2: Transcription Factor Binding Sites Within Upstream Regions of Genes Upregulated in Both Types of Senescence with log Fold Change > 2.0

ID	Yes density per 1000bp	No density per 1000bp	Yes-No ratio	Model cutoff	P-value
V$NKX25_Q6	0.03286	0.00306	10.73494	0.9931	0.0103
V$TBX5_Q2	0.03834	0.00612	6.26205	0.944	0.01296
V$RORALPHA_Q4	0.08215	0.0153	5.36747	0.9661	4.20E-04
V$MRF2_01	0.04929	0.01224	4.0256	0.9253	0.01494
V$SOX2_Q3_01	0.19168	0.06428	2.98193	0.9799	4.50E-05
V$CIZ_01	0.08215	0.03061	2.68373	0.999	0.0119
V$REVERBALPHA_Q6	0.06572	0.02449	2.68373	0.923	0.02388
V$TEF1_Q6_04	0.15882	0.06122	2.59428	0.9795	7.38E-04
V$ERALPHA_01	0.08762	0.03673	2.38554	0.8032	0.01741
V$SRF_Q5_02	0.06572	0.02755	2.38554	0.9202	0.03782
V$HNF4A_Q3	0.10405	0.04591	2.26627	0.9369	0.01346
V$HSF1_01	0.26287	0.1255	2.09462	0.9711	3.73E-04
V$ZSCAN4_04	0.31216	0.15917	1.96119	0.9276	3.27E-04
V$LEF1_Q5_01	0.38335	0.20202	1.89759	0.9966	1.40E-04
V$TATA_01	0.85433	0.46832	1.82424	0.9413	1.02E-07
V$STAT1_Q6	0.08215	0.04591	1.78916	0.9915	0.07897
V$ZFP105_04	0.33954	0.18978	1.78916	0.8666	8.66E-04
V$HNF6_Q4	0.43264	0.24181	1.78916	0.9235	1.88E-04
V$IRF1_Q5	0.12596	0.0704	1.78916	0.9829	0.03426
V$POU6F1_02	0.50383	0.28466	1.76992	0.8469	7.65E-05
V$PBX_Q3	0.38335	0.21732	1.76396	0.895	5.44E-04
V$E2A_Q6_01	0.19168	0.11019	1.73946	0.9844	0.01377
V$ETS_Q6	0.24096	0.14386	1.67496	0.999	0.00962
V$HIC1_08	0.15882	0.09489	1.67373	0.9737	0.03166
V$DLX3_02	0.15334	0.09183	1.66988	0.9955	0.03493
V$REST_Q5	0.16429	0.10101	1.62651	0.9123	0.03639
V$SF1_Q5_01	0.32859	0.20202	1.62651	0.96	0.00439
V$POU2F1_Q6	0.78861	0.49281	1.60024	0.9335	3.04E-05

V$CDX2_Q5_02	0.99671	0.62749	1.58842	1	4.18E-06
V$HNF1A_Q4	0.57503	0.36425	1.57867	0.8927	4.54E-04
V$PIT1_Q6_01	1.23768	0.8142	1.52011	0.9359	2.75E-06
V$RFX1_01	0.35049	0.23263	1.50666	0.9156	0.01031
V$DMRT4_01	0.16429	0.11019	1.49096	0.886	0.06862
V$AP1_Q6_02	1.5115	1.05601	1.43133	0.9099	6.43E-06
V$AIRE_01	0.50383	0.37343	1.3492	0.9046	0.01847
V$MEIS1_01	0.33406	0.24793	1.34739	0.9901	0.04794
V$CEBPA_Q6	1.47864	1.10193	1.34187	0.9733	1.69E-04
V$RELA_Q6	0.32859	0.24487	1.34187	0.9255	0.05176
V$GEN_INI_B	0.49836	0.37343	1.33453	0.9914	0.02267
V$BLIMP1_Q4	0.54217	0.41016	1.32184	0.9531	0.02136
V$CPHX_01	3.83899	2.92317	1.3133	0.7443	3.14E-08
V$GATA_Q6	1.22125	0.93358	1.30814	0.9789	0.00143
V$FPM315_01	0.47645	0.36425	1.30804	0.9362	0.03417
V$SIX1_01	3.35159	2.59259	1.29276	0.7544	8.94E-07
V$TBX5_01	0.77218	0.59994	1.2871	0.9	0.01334
V$ISL1_Q3	0.63527	0.49587	1.28112	0.9864	0.02474
V$MZF1_Q5	1.16648	0.91521	1.27455	0.9856	0.00411
V$ZNF333_01	2.11939	1.67432	1.26582	1	2.41E-04
V$DRI1_01	0.79956	0.63361	1.26192	1	0.01848
V$CRX_Q4_01	0.66265	0.52648	1.25865	1	0.03079
V$NF1_Q6	1.63198	1.31007	1.24572	0.9566	0.00215
V$HNF3B_Q6	0.79409	0.63973	1.24128	0.9678	0.02647
V$CDPCR1_01	4.89047	3.94245	1.24046	0.7788	4.99E-07
V$LRH1_Q5_01	0.56407	0.45914	1.22855	0.9727	0.062
V$RBPJK_01	0.72289	0.59076	1.22367	0.8594	0.04248
V$P53_Q3	1.35268	1.10805	1.22078	0.9531	0.00908
V$HOXC13_01	8.06134	6.61769	1.21815	0.7331	3.66E-09
V$CDX2_01	2.07558	1.70493	1.2174	0.831	0.00185
V$SOX10_Q3	0.96386	0.79278	1.2158	0.9811	0.0261
V$CP2_Q6	1.02957	0.85399	1.2056	0.982	0.02712
V$BBX_03	0.96933	0.80808	1.19955	0.8292	0.03469
V$IPF1_Q5	2.79299	2.34466	1.19121	0.9544	0.00128
V$AML3_Q6	0.7667	0.64585	1.18712	0.9256	0.06506
V$RUSH1A_02	3.08872	2.61096	1.18298	0.9765	0.00114
V$MAF_Q4	1.27054	1.07744	1.17922	0.8998	0.02881

V$HELIOSA_02	9.71522	8.24916	1.17772	0.7988	5.67E-08
V$DUXL_01	10.5586	8.99602	1.1737	0.6877	3.01E-08
V$MAFA_Q4	0.84337	0.71931	1.17247	0.9616	0.06971
V$XVENT1_01	2.15225	1.83961	1.16995	0.8503	0.00876
V$IRX2_01	21.30887	18.3165	1.16337	0.6537	1.48E-13
V$DBP_Q6	13.09419	11.37129	1.15151	0.8576	4.66E-08
V$NFAT1_Q4	1.25411	1.10193	1.1381	1	0.06891
V$HMX1_02	24.85761	21.92837	1.13358	0.6375	2.56E-11
V$NF1A_Q6_01	3.59255	3.17417	1.13181	0.9842	0.0072
V$HDX_01	26.24863	23.20784	1.13102	0.6804	1.67E-11
V$TTF1_Q5_01	2.14129	1.91919	1.11573	0.9771	0.04822
V$PAX_Q6	7.40964	6.65442	1.11349	0.7049	0.00105
V$PLZF_02	8.73494	7.85124	1.11256	0.6736	4.57E-04
V$HOXD12_01	12.15225	11.00092	1.10466	0.6761	1.26E-04
V$HOXB13_01	12.05367	10.94276	1.10152	0.7188	1.98E-04
V$HMGIY_Q3	4.91785	4.47505	1.09895	0.8627	0.014
V$FREAC3_01	3.41731	3.14662	1.08603	0.7484	0.05509
V$NANOG_01	10.96386	10.16223	1.07888	0.7318	0.00389
V$RHOX11_01	24.60022	23.1711	1.06168	0.683	7.86E-04

Table 3: Transcription Factor Binding Sites of Down-regulated genes with log Fold Change > 2.0 Threshold for Both Types of Cell Senescence.

ID	Yes density per 1000bp	No density per 1000bp	Yes-No ratio	Model cutoff	P-value
V$PBX_Q3	0.36932	0.01684	21.9375	0.9056	2.40E-05
V$DELTAEF1_01	0.14205	0.01684	8.4375	0.9921	0.02953
V$RHOX11_01	0.25568	0.05051	5.0625	0.9085	0.00892
V$TEF1_Q6_04	0.22727	0.05051	4.5	0.9801	0.01835
V$CPHX_01	0.51136	0.11785	4.33929	0.8487	4.37E-04
V$DEAF1_02	0.14205	0.03367	4.21875	0.8268	0.07171
V$IPF1_Q5	0.14205	0.03367	4.21875	0.9993	0.07171
V$SIX1_01	0.14205	0.03367	4.21875	0.8741	0.07171
V$CDX2_01	0.17045	0.05051	3.375	0.922	0.07142

V$BLIMP1_Q4	0.28409	0.08418	3.375	0.9698	0.01984
V$REST_Q5	0.3125	0.10101	3.09375	0.8913	0.01977
V$FPM315_01	1.02273	0.43771	2.33654	0.9421	6.80E-04
V$AIRE_01	0.3125	0.13468	2.32031	0.9064	0.05395
V$POU2F1_Q6	0.34091	0.15152	2.25	0.9355	0.05019
V$EGR1_Q6	0.25568	0.11785	2.16964	1	0.09564
V$ZSCAN4_04	0.25568	0.11785	2.16964	0.9108	0.09564
V$GFI1_Q6_01	0.3125	0.15152	2.0625	0.982	0.08049
V$CEBPA_Q6	1.13636	0.6229	1.82432	0.9729	0.00588
V$MAZR_01	0.39773	0.21886	1.81731	0.9453	0.08621
V$STAT1_Q6	0.42614	0.23569	1.80804	0.9678	0.0788
V$HSF1_01	0.48295	0.26936	1.79297	0.9646	0.06605
V$HNF3B_Q6	0.625	0.35354	1.76786	0.9627	0.04309
V$MZF1_Q5	2.64205	1.51515	1.74375	0.9774	1.20E-04
V$HIC1_08	0.59659	0.35354	1.6875	0.9496	0.06164
V$PIT1_Q6_01	0.51136	0.30303	1.6875	0.9362	0.08008
V$AP2ALPHA_03	0.85227	0.50505	1.6875	0.8904	0.02912
V$PLZF_02	3.77841	2.28956	1.65028	0.673	2.84E-05
V$CP2_Q6	1.07955	0.65657	1.64423	0.9823	0.01964
V$RUSH1A_02	0.99432	0.60606	1.64062	0.9925	0.02492
V$MAZ_Q6_01	6.07955	3.75421	1.61939	0.8848	3.52E-07
V$HOXB13_01	9.26136	5.77441	1.60386	0.709	8.14E-10
V$RNF96_01	0.53977	0.3367	1.60312	0.9757	0.09452
V$MUSCLEINI_B	0.9375	0.60606	1.54688	0.8956	0.04604
V$CDPCR1_01	2.72727	1.78451	1.5283	0.7979	0.00173
V$SRY_Q6	0.88068	0.58923	1.49464	0.9626	0.06653
V$TATA_01	1.5625	1.06061	1.47321	0.8673	0.02288
V$CDX2_Q5_02	0.90909	0.6229	1.45946	0.999	0.07471
V$FREAC3_01	1.81818	1.24579	1.45946	0.7499	0.01707
V$RREB1_01	4.48864	3.19865	1.40329	0.7482	0.00106
V$SP1_Q6_01	7.67045	5.55556	1.38068	0.9155	5.59E-05
V$PAX_Q6	3.09659	2.28956	1.35248	0.75	0.01156
V$NF1A_Q6_01	2.01705	1.49832	1.34621	0.9889	0.0375
V$GLI_Q3	13.60795	10.16835	1.33827	0.8804	1.31E-06
V$IK_Q5_01	13.18182	10.18519	1.29421	0.9357	1.88E-05
V$DUXL_01	5.28409	4.15825	1.27075	0.7031	0.00806
V$IRX2_01	10.65341	8.45118	1.26058	0.6563	4.21E-04

V$HOXC13_01	9.09091	7.23906	1.25581	0.6738	0.00122
V$GKLF_Q4	24.43182	19.7138	1.23933	0.9471	1.14E-06
V$CPBP_Q6	11.5625	9.44444	1.22426	1	0.00111
V$DBP_Q6	14.09091	11.53199	1.2219	0.8522	4.03E-04
V$HELIOSA_02	7.72727	6.44781	1.19843	0.7947	0.01277
V$HMX1_02	11.93182	10.15152	1.17537	0.6366	0.00622
V$HDX_01	8.92045	7.72727	1.15441	0.721	0.0276
V$P53_04	11.10795	9.88215	1.12404	0.7739	0.03974
V$ZIC1_05	23.18182	21.49832	1.07831	0.7075	0.04878

Four homeobox genes, namely IRX2, HMX1, HDH, HOXC13 were binders for Top sites enriched in genes overexpressed in both bleomycin induced and replicative senescence phenotypes, while HOXB13, MAZ, GKLF, GLI, IK, SP1, PLZF, PBX were among transcription factors that preferentially bind to the sites located in genes downregulated both in RS and in SIPS.

3.2 Genes Uniquely Involved in Replicative Senescence

A total of 1408 genes were upregulated and a total of 703 genes were downregulated in replicative senescence, but not in bleomycin induced senescence as compared to younger control fibroblasts. Functional analysis was performed for the lists of up- and downregulated genes separately, as described before.

The list of the signaling events significantly overrepresented in replicative senescence, but not in bleomycin induced senescence was represented entirely by various fragments

of cyclosome regulatory network (adjusted p-values range of <4.1e-5 to < 0.023), with top overrepresented being Aurora-B cell cycle regulation. The list of most significantly downregulated fragments centered around fatty acid anabolism, with an emphasis on the biosynthesis of n-9 MUFAs and PUFAs, cholesterol metabolism and biosynthesis of estrogens (adjusted p-value range of <5.8e-4 to < 0.028).

Upstream analysis aimed at identifying potential TFBSs overrepresented in the promoters of differentially expressed genes uniquely deregulated in replicative senescence was performed after filtration of gene expression levels by log fold change (FC) of 1.5 for up-regulated (N=1408 genes) and down-regulated (N=703) genes, separately.

The outputs are shown in the tables (4, 5). Interestingly, lists of putative transcription factor candidates for being positive drivers for replicative senescence was very similar to that driving both types of senescence. In particular, homeobox genes IRX2, HMX1, HOXB13, HOXC13 (p-values range of E-39 to < E-25) were among Top positive regulators of replicative senescence. The only non-homeobox positive regulator identified at similar levels of confidence was promyelocytic leukemia zinc finger PLZF (e-31). Transcription factors HOXB13, IRX2, PLZF, HDX, DUXL, CDX2 and CPXH were among these that significantly preferred to bind promoters of genes downregulated in replicative senescence (p-values range of E-23 to < E-12).

Table 4: Transcription Factor Binding Sites within Upstream Regions of Genes Upregulated in Replicative Senescence with log Fold Change > 1.5

ID	Yes density per 1000bp	No density per 1000bp	Yes-No ratio	Model cutoff	P-value
V$OSR1_03	0.03566	0.00306	11.6471	0.9927	0.008
V$ZBRK1_01	0.02377	0.00306	7.76471	0.9576	0.048
V$MAZR_01	0.13072	0.03673	3.55882	0.9628	2.49E-04
V$CIZ_01	0.16637	0.05204	3.19723	0.9988	1.01E-04
V$RORALPHA_Q4	0.04753	0.0153	3.10588	0.966	0.039
V$PBX_Q3	0.07724	0.02755	2.80392	0.9468	0.0139
V$DMRT4_01	0.2139	0.07652	2.79529	0.8964	5.56E-05
V$REVERBALPHA_Q6	0.06536	0.02449	2.66912	0.9244	0.0278
V$NF1A_Q6_01	0.23173	0.09489	2.44213	1	1.58E-04
V$HIC1_08	0.18419	0.09489	1.94118	0.9749	0.0067
V$HNF1A_Q4	0.6833	0.36731	1.86029	0.8921	1.67E-06
V$MYB_05	0.10695	0.05816	1.83901	0.9022	0.046
V$DLX3_02	0.16637	0.09183	1.81176	0.9955	0.0172
V$POU6F1_02	0.4694	0.26018	1.80415	0.8495	1.24E-04
V$BCL6_Q3_01	0.27332	0.15611	1.75087	0.9581	0.0043
V$IRF1_Q5	0.13072	0.07652	1.70824	0.9821	0.0469
V$REST_01	0.11884	0.0704	1.68798	0.8135	0.0604
V$GATA_Q6	1.37849	0.84481	1.63171	0.9841	3.50E-08
V$POU2F1_Q6	1.62805	1.00704	1.61666	0.8758	4.05E-09
V$ARID5A_03	1.52704	0.94582	1.61451	0.8788	1.29E-08
V$HSF1_01	1.05764	0.66728	1.585	0.9392	4.13E-06
V$HNF6_Q4	0.40404	0.26018	1.55294	0.9191	0.0047
V$PIT1_Q6_01	1.44385	0.94276	1.53151	0.933	5.60E-07
V$BBX_03	1.24183	0.8142	1.52521	0.829	3.91E-06
V$HSF1_02	0.2139	0.1408	1.51918	0.8377	0.0396
V$CDC5_01	0.3268	0.21732	1.50373	0.8522	0.0153
V$E2A_Q6_01	0.16043	0.10713	1.49748	0.9845	0.07489
V$ZNF333_01	2.46583	1.67432	1.47274	1	2.50E-09
V$CDX2_Q5_02	0.91503	0.62749	1.45825	1	2.83E-04

V$FPM315_01	0.54664	0.38261	1.42871	0.9348	0.00613
V$PLZF_02	11.2894	7.90328	1.42844	0.6731	1.17E-31
V$HMGIY_Q3	6.41711	4.53627	1.41462	0.8622	5.99E-18
V$LEF1_Q5_01	0.6833	0.48669	1.404	0.9954	0.0036
V$ISL1_Q3	0.68925	0.49587	1.38998	0.9864	0.0044
V$IPF1_Q5	3.16102	2.27426	1.38991	0.957	5.76E-09
V$AP1_Q6_02	2.50149	1.809	1.3828	0.9025	2.91E-07
V$XVENT1_01	3.74332	2.70891	1.38185	0.8341	4.91E-10
V$TATA_01	4.81283	3.48332	1.38168	0.856	2.04E-12
V$DRI1_01	0.87344	0.63361	1.37852	1	0.0019
V$HNF3B_Q6	1.78253	1.29783	1.37347	0.9559	1.85E-05
V$MAZ_Q6_01	0.94474	0.68871	1.37176	0.9234	0.00148
V$CDX2_01	2.26381	1.66208	1.36204	0.8322	2.77E-06
V$ZFP105_04	2.95306	2.18243	1.35311	0.7897	1.76E-07
V$CRX_Q4_01	0.70707	0.52648	1.34302	1	0.00838
V$SOX10_Q3	0.92692	0.69483	1.33402	0.9826	0.00352
V$BBX_04	2.48366	1.86716	1.33018	0.8125	4.98E-06
V$DBP_Q6	2.47178	1.87022	1.32165	0.9477	8.04E-06
V$STAT1_Q6	0.60606	0.46526	1.30263	0.9604	0.02347
V$CDPCR1_01	5.09804	3.94858	1.29111	0.7785	5.23E-09
V$FREAC3_01	3.64825	2.83747	1.28574	0.7542	9.68E-07
V$NFAT1_Q4	1.41414	1.10193	1.28333	1	0.00175
V$HMX1_02	28.4908	22.2987	1.27769	0.6363	3.45E-39
V$CEBPA_Q6	2.10933	1.68656	1.25067	0.9707	6.27E-04
V$HOXC13_01	23.5354	18.8307	1.24984	0.6625	1.11E-27
V$IRX2_01	22.5668	18.1757	1.24159	0.654	3.04E-25
V$HOXB13_01	32.246	25.978	1.24128	0.666	3.58E-35
V$DUXL_01	14.1474	11.5305	1.22696	0.6728	5.19E-15
V$SOX2_Q3_01	1.96078	1.60086	1.22483	0.9282	0.0023
V$RUSH1A_02	5.35948	4.38323	1.22272	0.9683	1.49E-06
V$CREBP1_01	5.29412	4.3618	1.21375	0.7391	3.74E-06
V$TEF1_Q6_04	1.31907	1.08968	1.21051	0.9039	0.0147
V$NKX25_Q6	1.17053	0.97337	1.20255	0.9584	0.024
V$SRY_Q6	1.86572	1.55494	1.19986	0.9626	0.0064
V$HOXD12_01	22.9531	19.1429	1.19903	0.6348	7.32E-19

V$HDX_01	26.322	22.0171	1.19553	0.6847	9.25E-21
V$HELIOSA_02	7.59358	6.41567	1.1836	0.8143	1.31E-06
V$CPHX_01	19.1622	16.2932	1.17608	0.6363	2.87E-13
V$MZF1_Q5	1.06952	0.91521	1.1686	0.9856	0.055
V$SIX1_01	17.9263	15.6902	1.14251	0.6493	4.19E-09
V$TTF1_Q5_01	2.19251	1.91919	1.14241	0.9771	0.0234
V$HOMEZ_01	21.7944	19.3541	1.12608	0.6385	6.72E-09
V$RHOX11_01	24.7534	22.8558	1.08302	0.6839	2.07E-05

Table 5: Transcription Factor Binding Sites of Down-Regulated genes with log Fold Change<- 1.5 Threshold for Replicative Cell Senescence

ID	Yes density per 1000bp	No density per 1000bp	Yes-No ratio	Model cutoff	P-value
V$DLX3_02	0.32362	0.0551	5.87371	0.9979	1.74E-08
V$OSR1_03	0.05178	0.00918	5.63876	0.9914	0.02856
V$FPM315_01	0.09061	0.01837	4.93392	0.9973	5.40E-03
V$BRCA_01	0.10356	0.02449	4.22907	1	5.27E-03
V$GCM2_01	0.07767	0.01837	4.22907	0.9563	0.01563
V$TBX5_01	0.03883	0.00918	4.22907	0.9957	0.08841
V$MYB_05	0.10356	0.03061	3.38326	0.9223	1.25E-02
V$HNF1A_Q4	0.32362	0.10101	3.20384	0.9207	0.0000245
V$AIRE_01	0.06472	0.02143	3.02077	0.9402	6.15E-02
V$CIZ_01	0.19417	0.07346	2.64317	0.9985	0.0039
V$SOX10_Q3	0.10356	0.03979	2.60251	0.9992	3.38E-02
V$SOX2_Q3_01	0.3754	0.14692	2.55506	0.9628	0.000115
V$PAX_Q6	0.19417	0.07958	2.43985	0.881	0.00671
V$ISL1_Q3	0.20712	0.08571	2.41661	0.9961	5.57E-03
V$DMRT4_01	0.4919	0.24793	1.98401	0.8637	0.0006
V$CDX2_01	3.15854	1.68962	1.86937	0.8314	4.88E-15
V$STAT1_Q6	0.90614	0.48669	1.86186	0.9589	0.0000225
V$HBP1_03	0.32362	0.18059	1.79198	0.9168	1.26E-02

V$HSF1_01	1.19092	0.66728	1.78475	0.9393	5.21E-06
V$PIT1_Q6_01	1.60516	0.90909	1.76567	0.9336	2.23E-07
V$NF1A_Q6_01	0.40129	0.22957	1.74802	0.9979	7.82E-03
V$HSF1_02	0.20712	0.11938	1.735	0.8545	0.04895
V$ARID5A_03	0.32362	0.18672	1.73323	0.9661	1.70E-02
V$CRX_Q4_01	0.89319	0.52648	1.69655	1	2.32E-04
V$POU6F1_02	0.80258	0.47444	1.69163	0.8321	0.000492
V$DRI1_01	1.06147	0.63361	1.67528	1	0.0000909
V$ZFP105_04	1.77344	1.06214	1.66969	0.8172	0.000000657
V$HNF3B_Q6	2.20062	1.33456	1.64895	0.9557	6.52E-08
V$CEBPA_Q6	2.3689	1.47536	1.60564	0.9718	9.29E-08
V$ZNF333_01	2.66663	1.67432	1.59267	1	2.54E-08
V$CPHX_01	9.21671	5.85246	1.57484	0.7141	1.27E-23
V$BBX_03	1.20387	0.76829	1.56695	0.8309	2.19E-04
V$HNF6_Q4	0.44012	0.29079	1.51356	0.903	0.02738
V$CP2_Q6	0.45307	0.30609	1.48018	0.994	0.03212
V$POU2F1_Q6	1.52749	1.06214	1.43813	0.8737	5.56E-04
V$HNF4A_Q3	0.47896	0.33364	1.43556	0.8845	3.89E-02
V$FREAC3_01	4.55658	3.22008	1.41505	0.7474	2.59E-08
V$HMGIY_Q3	6.74425	4.79951	1.4052	0.86	3.77E-11
V$BLIMP1_Q4	0.32362	0.23263	1.39114	0.9634	0.09742
V$HOXD12_01	3.22326	2.31711	1.39107	0.7496	6.53E-06
V$TEF1_Q6_04	1.39804	1.02234	1.36748	0.9059	0.00342
V$HOXB13_01	12.32347	9.02357	1.3657	0.7314	2.38E-16
V$ETS_Q6	0.73785	0.54178	1.3619	0.9871	2.80E-02
V$TATA_01	4.16823	3.07928	1.35364	0.8652	0.00000236
V$IPF1_Q5	2.71841	2.02326	1.34358	0.9576	0.00016
V$DUXL_01	10.34291	7.75941	1.33295	0.6971	2.86E-12
V$GATA_Q6	1.47571	1.10805	1.33181	0.9763	5.29E-03
V$PLZF_02	10.47236	7.92164	1.32199	0.673	7.85E-12
V$CDX2_Q5_02	1.42393	1.08968	1.30674	0.999	9.41E-03
V$NANOG_01	5.24265	4.02816	1.3015	0.7734	3.33E-06
V$GFI1_Q6_01	0.4919	0.37955	1.29601	0.9779	0.0985
V$SIX1_01	7.4821	5.78512	1.29334	0.7131	6.94E-08
V$XVENT1_01	2.42068	1.88246	1.28591	0.8498	1.81E-03

V$HMX1_02	28.2197	22.19773	1.27129	0.6366	3.90E-22
V$IRX2_01	23.65018	18.65932	1.26747	0.653	1.91E-18
V$LEF1_Q5_01	2.3689	1.87634	1.26251	0.961	3.75E-03
V$RELA_Q6	0.64724	0.51729	1.2512	0.9051	9.71E-02
V$HDX_01	30.0967	24.28834	1.23914	0.677	2.72E-19
V$PBX_Q3	1.37215	1.11417	1.23154	0.8503	3.55E-02
V$GEN_INI_B	2.20062	1.79982	1.22269	0.9704	1.29E-02
V$AP1_Q6_02	2.31712	1.89777	1.22097	0.9023	0.01146
V$NF1_Q6	1.56632	1.28864	1.21548	0.9571	0.03472
V$DBP_Q6	2.20062	1.81206	1.21443	0.9479	0.0155
V$HOXC13_01	16.81532	13.89042	1.21057	0.6871	1.33E-09
V$HIC1_08	1.82522	1.50903	1.20953	0.9014	2.76E-02
V$CDPCR1_01	4.6213	3.87818	1.19162	0.7807	2.16E-03
V$NFAT1_Q4	1.30743	1.10193	1.18649	1	7.37E-02
V$RUSH1A_02	4.66013	4.00061	1.16486	0.9694	0.00617
V$CREBP1_01	5.30737	4.57606	1.15981	0.7291	4.67E-03
V$MYB_Q4	3.24915	2.8038	1.15884	0.9675	0.02215
V$IK_Q5_01	2.67958	2.32935	1.15035	0.9765	0.04171
V$MAFA_Q4	2.34301	2.08448	1.12403	0.9595	0.08873
V$HELIOSA_02	11.36555	10.18365	1.11606	0.7827	2.20E-03
V$TTF1_Q5_01	3.54688	3.2262	1.0994	0.9674	8.74E-02
V$RHOX11_01	25.29417	23.52005	1.07543	0.682	0.00226
V$HOMEZ_01	13.44966	12.56198	1.07066	0.6633	0.02626

3.3 Genes Uniquely Involved in Bleomycin-Induced Senescence

A total of 1408 genes were upregulated and a total of 703 genes were downregulated in replicative senescence, but not in bleomycin induced senescence as compared to younger control fibroblasts. Functional analysis was performed for the lists of up- and downregulated genes separately, as described before.

The list of the signaling events significantly overrepresented in replicative senescence, but not in bleomycin induced senescence was represented entirely by various fragments of cyclosome regulatory network (adjusted p-values range of <4.1e-5 to < 0.023), with Top overrepresented being Aurora-B cell cycle regulation. The list of most significantly downregulated fragments centered around fatty acid anabolism, with an emphasis on biosynthesis of n-9 MUFAs and PUFAs, cholesterol metabolism and biosynthesis of estrogens (adjusted p-value range of <5.8e-4 to < 0.028).

Upstream analysis aimed at identifying potential TFBSs overrepresented in the promoters of differentially expressed genes uniquely deregulated in replicative senescence was performed after filtration of gene expression levels by log fold change (FC) of 1.5 for up-regulated (N=1408 genes) and down-regulated (N=703) genes, separately.

The outputs are shown in the tables (6, 7). Interestingly, lists of putative transcription factor candidates for being positive drivers for replicative senescence was very similar to that driving both types of senescence. In particular, homeobox genes IRX2, HMX1, HOXB13, HOXC13 (p-values range of E-39 to < E-25) were among Top positive regulators of replicative senescence. The only non-homeobox positive regulator identified at similar levels of confidence was promyelocytic leukemia zinc finger PLZF (e-31). Transcription factors HOXB13, IRX2, PLZF, HDX, DUXL, CDX2 and CPXH were among these that significantly preferred to bind promoters of genes downregulated in replicative senescence (p-values range of E-23 to < E-12).

Table 6: Transcription Factor Binding Sites within Upstream Regions of Genes Upregulated in Bleomycin Induced Senescence with Log Fold Change > 1.5

ID	Yes density per 1000bp	No density per 1000bp	Yes-No ratio	Model cutoff	P-value
V$HMGA2_01	0.03418	0.00612	5.58271	0.9052	0.03286
V$NKX25_Q6	0.03418	0.00612	5.58271	0.992	0.03286
V$ZSCAN4_04	0.04785	0.00918	5.21053	0.9798	1.27E-02
V$HMGIY_Q3	0.07519	0.01837	4.09398	0.9715	4.22E-03
V$TBX5_Q2	0.03418	0.00918	3.7218	0.9374	0.06551
V$REVERBALPHA_Q6	0.08886	0.02449	3.62876	0.9218	0.0033
V$REST_Q5	0.08202	0.02449	3.34962	0.9278	6.75E-03
V$HNF3B_Q6	0.38961	0.13468	2.89286	0.9866	9.97E-08
V$RORALPHA_Q4	0.08202	0.03061	2.6797	0.9634	1.80E-02
V$ZFP105_04	0.08886	0.03367	2.6391	0.9252	0.01505
V$RELA_Q6	0.59467	0.22957	2.59038	0.9269	1.54E-09
V$GCM2_01	0.06152	0.02449	2.51222	0.9497	0.04853
V$MEF2_03	0.10936	0.04591	2.38195	0.8994	0.01302
V$CIZ_01	0.17088	0.07346	2.32613	0.9985	2.64E-03
V$SOX2_Q3_01	0.30075	0.14692	2.04699	0.963	0.000511
V$HSF1_02	0.06835	0.03367	2.03008	0.8779	0.08121
V$SRF_Q5_02	0.06152	0.03061	2.00977	0.9182	0.09908
V$XVENT1_01	0.34176	0.17141	1.99382	0.9143	3.35E-04
V$HSF1_01	0.32809	0.17447	1.88049	0.9682	1.03E-03
V$IRF1_Q5	0.12987	0.0704	1.84472	0.9824	3.59E-02
V$E2A_Q6_01	0.84074	0.47138	1.78357	0.9766	1.68E-06
V$INSM1_01	0.12987	0.07346	1.76786	0.9181	0.04605
V$HNF1A_Q4	0.22556	0.13162	1.71376	0.9179	1.45E-02
V$COE1_Q6	0.35543	0.21732	1.6355	0.9547	5.14E-03
V$POU6F1_02	0.55366	0.33976	1.62955	0.841	0.000645
V$CDPCR1_01	1.0458	0.64891	1.61161	0.8441	6.09E-06

V$FPM315_01	0.93643	0.59382	1.57697	0.9217	3.71E-05
V$PBX_Q3	0.78606	0.49893	1.57549	0.8738	1.50E-04
V$AIRE_01	0.21189	0.13468	1.57331	0.9164	3.64E-02
V$TBX5_01	0.51265	0.32752	1.56524	0.9566	0.00214
V$BCL6_Q3_01	0.21189	0.13774	1.53835	0.9593	4.37E-02
V$TTF1_Q5_01	0.30759	0.20508	1.49983	0.9997	2.37E-02
V$ERALPHA_Q6_01	0.15721	0.10713	1.46745	1	0.09928
V$ZIC1_05	0.25974	0.17753	1.46305	0.9133	0.04449
V$CP2_Q6	1.30554	0.90603	1.44094	0.9812	6.32E-05
V$CDX2_01	1.0663	0.74992	1.42188	0.8628	4.22E-04
V$PIT1_Q6_01	1.13465	0.7989	1.42027	0.9363	2.95E-04
V$MAFA_Q4	0.67669	0.48056	1.40812	0.9978	5.09E-03
V$AP1_Q6_02	2.62474	1.8641	1.40805	0.9024	1.35E-07
V$POU2F1_Q6	0.6972	0.49893	1.39739	0.9333	5.31E-03
V$HNF6_Q4	0.36227	0.26018	1.39239	0.9191	0.03712
V$MZF1_Q5	1.05947	0.76217	1.39007	0.9887	8.85E-04
V$BLIMP1_Q4	0.45796	0.33058	1.38534	0.9569	2.30E-02
V$RBPJK_01	0.73821	0.53872	1.3703	0.8626	0.00646
V$BBX_03	0.92276	0.68871	1.33985	0.8353	0.00463
V$TEF1_Q6_04	1.65414	1.23661	1.33764	0.9	2.38E-04
V$LEF1_Q5_01	1.43541	1.07744	1.33224	0.9807	6.71E-04
V$IPF1_Q5	0.73821	0.56321	1.31072	0.9909	0.01581
V$MAF_Q4	1.52427	1.17539	1.29682	0.8977	1.30E-03
V$GATA_Q6	1.51059	1.16621	1.29531	0.9745	1.42E-03
V$ETS_Q6	1.3944	1.10499	1.26191	0.9779	0.00486
V$SOX10_Q3	1.38072	1.09581	1.26001	0.976	5.28E-03
V$EBOX_Q6_01	3.33561	2.67218	1.24828	0.901	5.80E-05
V$SRY_Q6	1.43541	1.1509	1.2472	1	6.26E-03
V$MYOGENIN_Q6_01	1.18934	0.96113	1.23744	1	1.44E-02
V$NF1A_Q6_01	2.1121	1.73248	1.21912	0.9889	3.06E-03
V$MEIS1_01	0.62201	0.51423	1.20959	0.9853	8.23E-02
V$CEBPA_Q6	5.85099	4.84848	1.20677	0.9506	6.28E-06
V$DELTAEF1_01	1.12098	0.93052	1.20469	0.9788	3.14E-02
V$STAT1_Q6	0.71087	0.59382	1.19712	0.9504	7.89E-02
V$HIC1_08	1.77033	1.4876	1.19006	0.9023	0.01367

V$DUXL_01	13.82092	11.61922	1.18949	0.6724	2.3E-10
V$HELIOSA_02	11.79084	9.99082	1.18017	0.7844	1.88E-08
V$LRH1_Q5_01	0.82023	0.69789	1.17531	0.9643	8.54E-02
V$CDX2_Q5_02	1.27136	1.08968	1.16672	0.999	4.95E-02
V$PAX_Q6	7.79904	6.71258	1.16185	0.7045	2.46E-05
V$IRX2_01	15.49556	13.40986	1.15553	0.6668	1.59E-08
V$DBP_Q6	12.48804	10.85399	1.15055	0.8649	7.21E-07
V$IK_Q5_01	2.66576	2.32935	1.14442	0.9765	1.69E-02
V$CPHX_01	17.1702	15.00765	1.1441	0.6393	2.75E-08
V$RUSH1A_02	5.02392	4.39241	1.14377	0.9682	0.00175
V$FAC1_01	2.89815	2.55586	1.13392	0.8781	0.0194
V$HDX_01	26.07656	23.05479	1.13107	0.681	3.97E-10
V$NF1_Q6	1.6473	1.45699	1.13062	0.9549	6.59E-02
V$NFAT1_Q4	1.24402	1.10193	1.12895	1	0.09953
V$SIX1_01	15.42037	13.69146	1.12628	0.6593	2.53E-06
V$TATA_01	3.86876	3.46495	1.11654	0.8564	0.01764
V$NANOG_01	10.78606	9.68779	1.11337	0.734	0.000281
V$GEN_INI_B	3.92344	3.56596	1.10025	0.9608	0.03284
V$HOXB13_01	7.71702	7.0401	1.09615	0.7439	6.26E-03
V$HMX1_02	17.42994	16.24426	1.07299	0.6626	1.86E-03
V$RHOX11_01	24.8257	23.23845	1.0683	0.6828	0.000571
V$HOXC13_01	18.94053	17.98286	1.05325	0.6665	0.01273

Table 7: Transcription Factor Binding Sites of Down-Regulated Genes with Log Fold Change <- 1.5 Threshold for Bleomycin Induced Cell Senescence

ID	Yes density per 1000bp	No density per 1000bp	Yes-No ratio	Model cutoff	P-value
V$REVERBALPHA_Q6	0.02256	0.00306	7.36917	0.9674	0.07585
V$HNF3B_Q6	0.10526	0.02143	4.91278	0.9917	0.000375
V$XVENT1_01	0.07519	0.01837	4.09398	0.9421	5.36E-03
V$ERALPHA_01	0.12782	0.03673	3.47989	0.8075	8.12E-04
V$STAT1_Q6	0.06015	0.02143	2.8073	0.9943	0.0408
V$RORALPHA_Q4	0.08271	0.03061	2.70203	0.9633	0.02015
V$DLX3_02	0.22556	0.09183	2.45639	0.9955	4.70E-04
V$HBP1_03	0.17293	0.0704	2.45639	0.9517	0.00208
V$SOX2_Q3_01	0.32331	0.13468	2.40056	0.9643	4.47E-05
V$MAZR_01	0.33083	0.16223	2.03927	0.9431	0.000434
V$REST_01	0.09774	0.04897	1.99582	0.8257	5.01E-02
V$NF1A_Q6_01	0.18797	0.09489	1.98096	1	0.00893
V$CIZ_01	0.12782	0.06734	1.89812	0.9986	0.03614
V$SIX1_01	0.24812	0.13774	1.80135	0.8634	7.97E-03
V$POU6F1_02	0.45113	0.2663	1.69406	0.8489	0.00135
V$CTCF_01	0.11278	0.06734	1.67481	0.9002	0.08716
V$HNF1A_Q4	0.33835	0.20202	1.67481	0.9089	0.00578
V$LEF1_Q5_01	0.33835	0.20202	1.67481	0.9966	5.78E-03
V$ZSCAN4_04	0.6015	0.36119	1.66535	0.8951	3.58E-04
V$EKLF_Q5_01	0.18797	0.11325	1.65972	0.9901	3.59E-02
V$MAZ_Q6_01	2.86466	1.76921	1.61918	0.8881	5.26E-13
V$INSM1_01	0.14286	0.08877	1.60936	0.916	0.07384
V$DMRT4_01	0.3985	0.25406	1.56854	0.8607	7.54E-03
V$GKLF_Q4	3.13534	2.01714	1.55435	0.9989	2.98E-12
V$CDX2_01	0.34586	0.22345	1.54786	0.9017	0.01422
V$FPM315_01	0.83459	0.54484	1.53179	0.9245	0.000333
V$SRF_Q5_02	0.18045	0.11938	1.51163	0.884	0.07398
V$RFX1_01	0.66917	0.44383	1.50772	0.9014	1.69E-03

V$PIT1_Q6_01	0.69173	0.45914	1.50659	0.9511	1.46E-03
V$MZF1_Q5	1.99248	1.32844	1.49987	0.9774	2.03E-07
V$RNF96_01	1.90226	1.28558	1.47968	0.8908	8.10E-07
V$BBX_03	0.2406	0.16529	1.45564	0.8921	6.02E-02
V$HNF4A_Q3	0.30075	0.20814	1.44494	0.9063	0.04223
V$GFI1_Q6_01	0.44361	0.31221	1.42085	0.9797	0.02081
V$E2A_Q6_01	0.63158	0.44689	1.41327	0.9768	7.74E-03
V$CP2_Q6	0.44361	0.3214	1.38026	0.9939	3.03E-02
V$COE1_Q6	0.32331	0.23569	1.37175	0.9543	6.07E-02
V$LRH1_Q5_01	0.26316	0.19284	1.36466	0.9828	8.73E-02
V$PBX_Q3	3.08271	2.30793	1.3357	0.8277	1.95E-06
V$RBPJK_01	0.93985	0.70401	1.335	0.8498	6.02E-03
V$SP1_Q6_01	3.56391	2.67218	1.33371	0.9072	3.83E-07
V$CPHX_01	2.24812	1.71717	1.3092	0.758	1.19E-04
V$HSF1_01	1.06767	0.82032	1.30152	0.9368	7.02E-03
V$RHOX11_01	0.91729	0.70707	1.29731	0.8719	0.01245
V$SOX10_Q3	0.78195	0.603	1.29677	0.9838	0.0197
V$DBP_Q6	3.54887	2.75482	1.28824	0.9371	6.25E-06
V$DRI1_01	0.81203	0.63361	1.2816	1	2.23E-02
V$GCM2_01	0.54135	0.42241	1.2816	0.8949	0.05272
V$GATA_Q6	1.37594	1.07438	1.28068	0.9784	4.20E-03
V$CDPCR1_01	2.43609	1.91919	1.26933	0.8099	3.27E-04
V$HIC1_08	1.90977	1.50903	1.26556	0.9014	0.00147
V$ISL1_Q3	0.62406	0.49587	1.25852	0.9864	5.24E-02
V$MYOGENIN_Q6_01	1.18797	0.96113	1.23602	1	1.77E-02
V$RREB1_01	1	0.8142	1.2282	0.7974	3.10E-02
V$IPF1_Q5	1.65414	1.36211	1.2144	0.9628	1.09E-02
V$POU2F1_Q6	1.16541	0.96113	1.21255	0.8776	2.89E-02
V$EGR1_Q6	1.33835	1.10499	1.21118	0.9123	2.13E-02
V$IRX2_01	3.04511	2.52219	1.20733	0.776	0.00117
V$TEF1_Q6_04	1.4812	1.23049	1.20375	0.9002	1.92E-02
V$P53_Q3	1.36842	1.1509	1.189	0.9521	3.16E-02
V$GLI_Q3	6.3609	5.39333	1.1794	0.8868	5.07E-05
V$DUXL_01	6.27068	5.41169	1.15873	0.7159	0.000273

V$CHCH_01	1.12782	0.97337	1.15867	1	0.07634
V$AP1_Q6_02	1.21805	1.05601	1.15344	0.9099	7.44E-02
V$BEN_01	8.84211	7.7288	1.14405	0.8701	8.35E-05
V$CPBP_Q6	6.31579	5.53719	1.14061	1	9.45E-04
V$NANOG_01	4.73684	4.15978	1.13872	0.7719	4.00E-03
V$IK_Q5_01	12.81203	11.25497	1.13834	0.9265	6.14E-06
V$HDX_01	6.81955	6.1157	1.11509	0.7625	3.63E-03
V$ZIC1_05	21.99248	20.73768	1.06051	0.6973	0.0042
V$HMX1_02	17.37594	16.48913	1.05378	0.6617	0.01838

3.4 Master Regulators of Replicative and Bleomycin-Induced Senescence

An analysis of DEGs upregulated in RS and in SIPS identified stromelysin and MGAT1 as master regulator molecules that influence the replicative senescence and bleomycin–induced senescence expression programs, respectively.

3.5 Bridging Senescence Regulators to Ospeopontin Secretion

In their previous publication, Pazolli et al. (2009) identified SPP1-encoded osteopontin as a secreted driver for tumor cells growth that is provided by senescent fibroblast [12]. To understand how senescence-wide targets highlighted by microarray analysis of senescent fibroblasts results in an increase in osteopontin secretion, a concise network was constructed using Shortest Path function in Pathway Studio software (Figure 3). Iroquois Homeobox 2 (IRX2) and POU4F1 were highlighted as most plausible connecting signaling molecules.

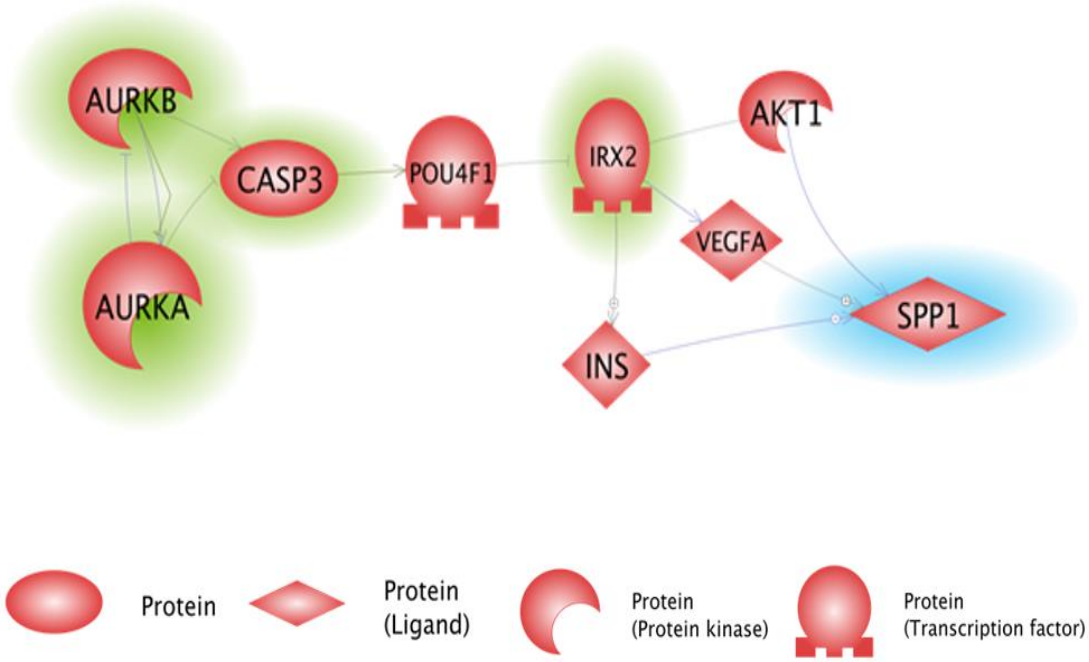

Figure 3: Pathway Studio Guided Network

Pathway Studio guided network that describes regulatory connections between the de-regulation of Aurora kinases, caspase-3 and osteopontin-encoding *SPP1*. Genes that were highlighted by either analysis of DEGs or by analysis of TFBS are highlighted in green. The gene of interests, SPP1, is highlighted in blue.

4. **DISCUSSION**

Over past decade, transcriptome profiling efforts that employ either microarray or RNAseq have already generated enormous amounts of data, with respective data analysis often only scratching the surface [20, 21]. In many cases, high-quality datasets are generated to investigate specific hypothesis, and consequently, these datasets get analyzed in a particular way. At least in theory, the study design of these narrow-set, but technically sound experiments should allow extraction of additional information that could remain unrecovered at the moment that the main manuscript gets sent to the publishers [22].

In their 2009 paper, Pazolli et al. started to investigate the mechanisms of the manner in which senescent BJ fibroblasts stimulate the growth of preneoplastic cells in vitro and in vivo [12]. In their experiments, replicative senescent (RS) and stress-induced premature senescent (SIPS) fibroblasts were equally proficient at inducing the growth of HaCaT cells. Their study of fibroblasts/HaCaT xenografts in vivo arrived essentially at same results [12]. The authors subsequently hypothesized that growth-promoting activities of both types of senescent cells are maintained by a common core of genes. Based on that hypothesis, they embarked on microarray-driven dissection of secreted factors commonly produced by RS and SIPS fibroblasts. After a set of validation experiments in qRT-PCR

and in-cell cultures, soluble protein osteopontin was highlighted as the protein of functional importance, and its gene, SPP1, was identified as a master regulator of a cancer niche environment [12]. An objective of the study achieved; however, the microarray dataset never got analyzed in larger context, i.e. for the purpose of direct comparison between RS and SIPS drivers.

In this study, we used the dataset of Pazolli et al., 2009 to extract the differentially expressed genes (DEGs) that differentiate the processes of RS and SIPS, to reconstruct relevant molecular cascades and to gain additional insights into popular cellular model of the bleomycin induced senescence. Analysis of signaling events indicated that an involvement of caspase-3/keratin-18 pathway that is indicative of apoptotic rather than necrotic cell death [23] and an evolutionarily conserved serine/threonine kinase Aurora A/ MDM2 pathway essential for mitotic progression [24] was shared between both types of senescence. Observed upregulation of Aurora A is consistent with the previously demonstrated increase in a number of aneuploid cells observed in aging fibroblast cultures [25]. Our analysis also highlighted concerted alteration of glutamate, polyamine and choline metabolisms as well as wnt/β-catenin and SDF-1/CXCL12 cascades. All these findings are generally consistent with previous studies of various aging fibroblasts both in culture and in human cohorts [26-28]. This consistency prompts us to stress on the high quality of the dataset of Pazolli et al., 2009 being analyzed.

An analysis aimed at identifying master regulator molecules that influence the replicative senescence and bleomycin–induced senescence expression programs, pointed at stromelysin/MMP3 and N-acetylglucosaminyltransferase enzyme MGAT1 that initiates the synthesis of hybrid and complex N-glycans as key orchestrating components in replicative senescence and in bleomycin-induced senescence, respectively (Figure 4 and Figure 5). Traditionally, MMP3 is seen as end-point biomarker or effector molecule associated with aging in fibroblasts. However, in Hutchinson-Gilford progeria syndrome, there is a progressive loss of MMP3 mRNA and protein expression [29]. Another study linked carrier status for MMP3 6A (rs3025058) allele to skin and lung aging [30]. Moreover, an exposure to MMP3 stimulates expression of Rac1b, a tumor-associated protein with cell-transforming properties that aids in bypassing replicative senescence [31] while driving motility and protumorigenic responses of the stroma [32]. Hence, there is an accumulation of evidence that stresses on an importance of MMP3 as a molecule of importance in replicative senescence that deserves additional investigations. An identification of MGAT1 that controls the synthesis the complex N-glycan sugars in the Golgi as the key regulator of SIPS is even more intriguing as there are strong associations between human plasma N-glycans and age [33, 34].

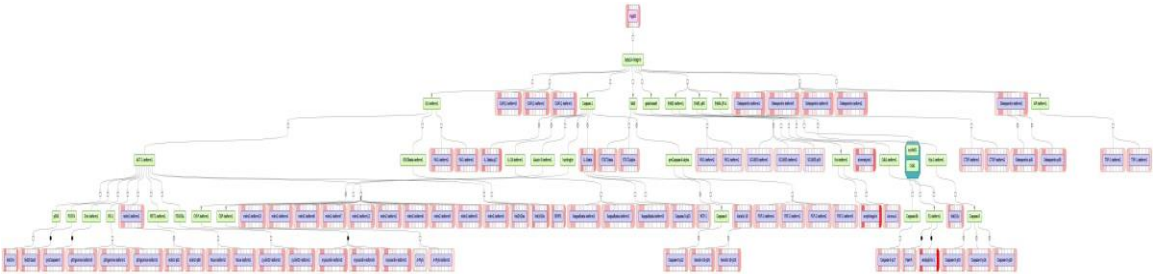

Figure 4: MGAT Master Molecule

Compiled output of an analysis for master regulators orchestrating gene expression program executed in replicative senescence and stress-induced senescence. MGAT, the master regulator of this network, is highlighted in red, intermediate controllers that are added by GeneXPlain algorithm, a subset of input molecules is highlighted in blue. The intensity of the pink/red bars on a side of the molecule box represents the degree of overexpression for respective genes.

The specific question was aimed to dissect the differences of the senescence programs executed in SIPS and RS. Indeed, the analysis showed that in RS fibroblasts, the list top deregulated events are populated by fragments of Aurora-B driven cell cycle signaling that are accompanied by the suppression of anabolic branches of the fatty acids and estrogen metabolism. This may be interpreted as an execution of ordered senescence program that proceeds along with shutting down the metabolism on a way to the halt of mitotic progression and apoptosis that is being upregulated in both RS and SIPS. On the other end, in bleomycin exposed fibroblasts, Aurora-B signaling is deprioritized and the synthetic branches of cholesterol metabolism are upregulated, rather than downregulated, while proteasome/ ubiquitin ligase pathways of protein degradation are dominating the regulatory landscape. This picture is indicative that the cells are going down actively fighting overwhelming amounts of stress that is facilitating premature senescence of

cells, but fail to completely activate orderly program of replicative senescence. Latter observation is consistent with activation of 26S proteasome and enhanced protein polyubiquitination previously observed in both idiopathic and bleomycin-induced pulmonary fibrosis [35]. Generalized mechanistic depiction of cellular processes common and differentiating RA and SIPS is presented in Figure 5.

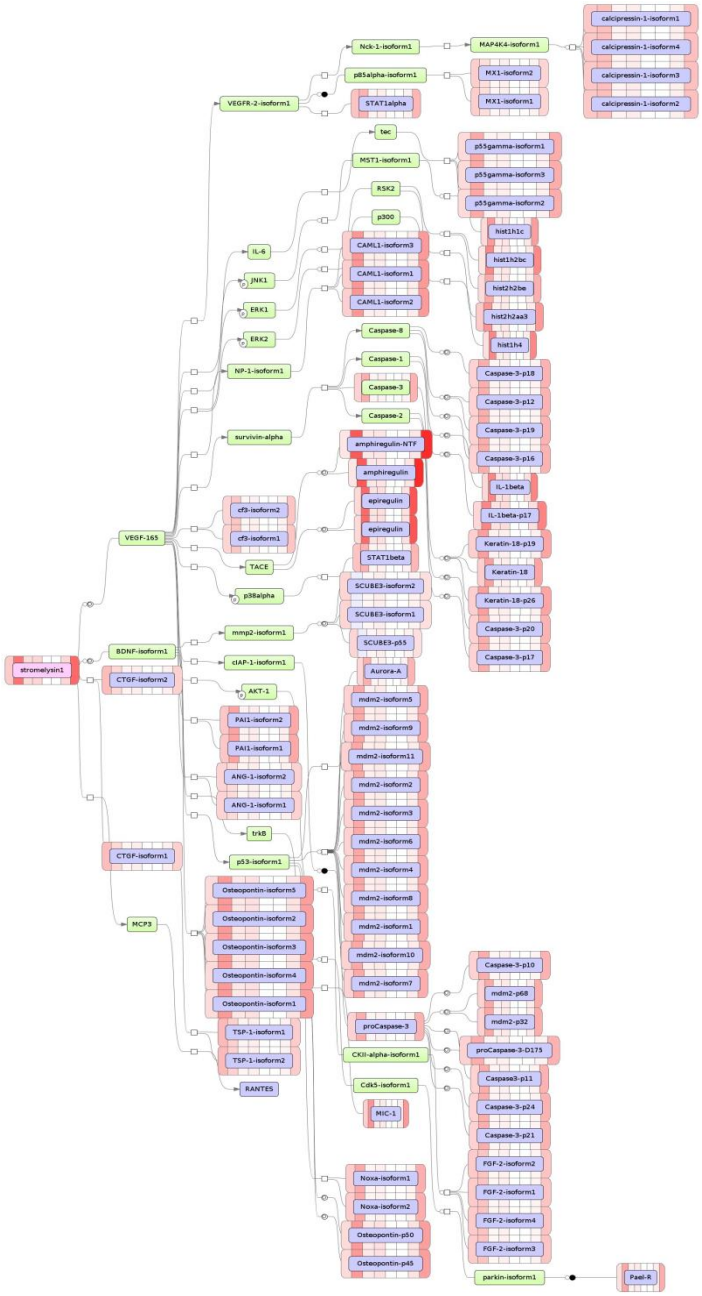

Figure 5: Hierarchically compiled output of a Master Molecule of Both Types of Senescence Stromelysin

Hierarchically compiled output of an analysis for master regulators orchestrating gene expression program executed in replicative senescence. Stromelysin, the master regulator of this network, is highlighted in red, intermediate controllers that are added by GeneXPlain algorithm, a subset of input molecules is highlighted in blue. The intensity of the pink/red bars on a side of the molecule box represents the degree of overexpression for respective genes.

The list of the transcription factors capable of binding to the promoter regions of the genes that change their expression in either RS or SIPS was unusually enriched by the members of homeobox family, with particular emphasis on HMX1, IRX2, HDX and HOXC13. The possibility of an involvement of homeobox genes in aging has been proposed earlier [36], with many homeobox containing TFs included in manually curated GenAge reference database [37]. Our findings indicate that the senescent program may be orchestrated by transcription factors (TFs) of Homeobox family at least in the case of replicative senescence in vitro. On the other hand, promoters of genes that change their expression in bleomycin-induced senescence but not in replicative senescent fibroblasts were enriched by binding sites for transcription factors Ikaros, RelA, HNF3B, GKLF and MAZ. Both RelA and GKLF are known stress-induced transcription regulators. RelA is the central player in the classical (or canonical) pathway of induction of NF-κB subunits that promotes senescence when activated in human lung fibroblasts exposed to ROS [38]. GKLF-deficient fibroblasts exposed to excessive levels of reactive oxygen species are more prone to become prematurely senescent than normal fibroblasts [39]. Moreover, yet another transcription factor, HNF3B/FOXA2 is epigenetically silenced in peroxide-stressed fibroblasts [40], therefore, an enrichment for binding sites for this factor in transcripts downregulated in bleomycin induced senescence is not surprising.

SPP1-encoded osteopontin, a secreted stromal driver for tumor growth, is overexpressed by both RS and SIPS fibroblasts [12]. The concise network constructed using Shortest Path function in Pathway Studio software (Figure 3) highlighted Iroquois Homeobox 2

(IRX2) and POU4F1 were highlighted as most likely signaling events to connect the DEGs identified by GeneXPlain-guided microarray analysis and osteopontin. In this network, suppression of Aurora kinases that normally monitor the mitotic checkpoint, centrosome separation and cytokinesis, cause catastrophic consequences and result in an increase in apoptosis, thus, being in in agreement with recently published observations of senescent fibroblasts [41]. Apoptosis activated caspase-3 directly or indirectly eliminates POU4F1/Brn-3a, the prediction that is consistent with previous observation of enhanced apoptosis in the neurons derived from Brn-3a knockout mice [42]. Moreover, POU4F1 gene is expressed in fibroblasts where it is required for proliferation, and cooperates with activated RAS/RAF signaling by reducing oncogene-induced senescence, consistent with its caspase-driven downregulation in both RS and SIPS [43]. In our network, POU4F1/Brn-3a suppresses transcription factor IRX2 that repeatedly showed up in lists of TF that recognize bindings sites differentially enriched in promoters of genes associated with fibroblast senescence. Caspase-3-driven removal of POU4F1 allows higher levels of IRX2 biosynthesis that is known for its ability to upregulate VEGF, metalloproteinases and other secreted molecules [44, 45].

An involvement of IRX2 in the transcription of osteopontin-encoding SPP1 gene was never evaluated in wet lab experiments; however, the knowledge-based algorithm identified IRX2 as a positive regulator of SPP1 expression by three independent molecular interaction events involving AKT1, VEGFA and INS. Moreover, marker co-expression pattern of IRX2 and SPP1 was observed during hair-cell development in the

chick's cochlea [46]. Two independent studies demonstrated that an expression of IRX2 is commonly suppressed by DNA methylation of its promoter [47, 48], including its differential methylation noted in osteoarthritis and osteoporosis [49], two age-related diseases of the cartilage and the bone characterized by changes in the levels of osteopontin secretion [50, 51]. As IRX2 is expressed strongly in human primary osteoblasts of the skeleton [52], its putative roles in SPP1 regulation in osteoarthritis and osteoporosis are worthy of investigation.

Importantly, Pazolli and co-authors followed up on their own study that identified osteopontin as a driver of tumor cell proliferation supplied by senescent stromal fibroblasts [12] and showed that the treatment with histone deacetylase (HDAC) inhibitors that reverse CpG methylation is sufficient to induce expression of osteopontin [53]. Moreover, an examination of PWM matches in the promoter of SPP1 showed that it contains 25 sites for IRX2 binding within 1100 nucleotides located between positions -1000 to +100 relative to major transcription start site (TSS) for SPP1 gene (Figure 6).

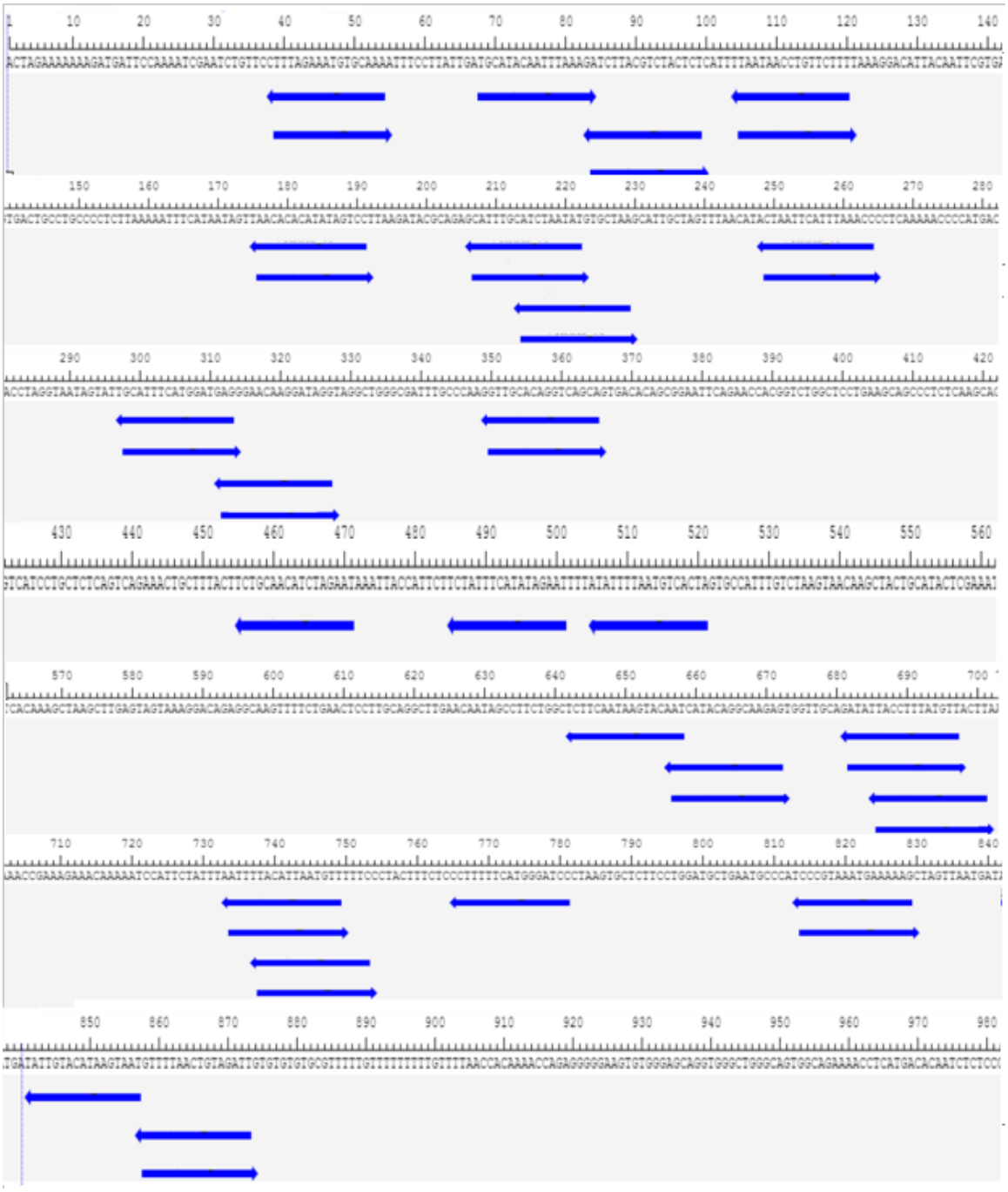

Figure 6: IRX2 Binding sites in Osteopontin (SPP1) Gene

Gene: SPP1 ENSG00000118785 TSS 88896866
chr4:88,895,867-88,896,966
secreted phosphoprotein 1 [Source:HGNC Symbol;Acc:HGNC:11255]
Synonyms: BSPI, BNSP, OPN, ETA-1
IRX2 sites are shown as blue arrows in this figure.

All this evidence adds up in favor of the hypothesis that SPP1/osteopontin expression might be controlled by IRX2, and that its derepression in senescent fibroblasts aid in SIPS-dependent stromal activation that, in turn, stimulate the growth of tumor cells.

5. CONCLUSION

A detailed comparison of stress/bleomycin induced and replicative senescence has been presented in this thesis. The master regulatory molecules and transcription factors which play a key role in these two types of cell senescence, RS and SIPS has been presented. It was shown that SIPS proceeds in cells that are actively fighting stress which facilitates premature senescence while failing to completely activate the orderly program of RS. Stromelysin/MMP3 and MGAT1 were identified as master regulators of RS and SIPS, respectively. This thesis also demonstrated that the promoters of genes differentially expressed in either RS or SIPS are unusually enriched by the binding sites for homeobox family proteins. Moreover, Iroquois Homeobox 2 (IRX2) was highlighted as a master regulator for the secretion of SPP1-encoded osteopontin, which is a stromal driver for tumor growth that is overexpressed by both RS and SIPS fibroblasts. The latter supports the hypothesis that senescence-specific de-repression of SPP1 aids in SIPS-dependent stromal activation.

REFERENCES

1. Santos Franco S, Raveh-Amit H, Kobolák J, Alqahtani MH, Mobasheri A, Dinnyes A. The crossroads between cancer stem cells and aging. BMC Cancer. 2015;15 Suppl 1:S1.

2. Hayflick L. The limited in vitro lifetime of human diploid cell strains. Exper. Cell Res. 1965; 37:614–636.

3. Shay JW, Wright WE. Hayflick, his limit, and cellular ageing. Nat Rev Mol Cell Biol. 2000;1(1):72-6.

4. Salama R, Sadaie M, Hoare M, Narita M. Cellular senescence and its effector programs. Genes Dev. 2014;28(2):99-114.

5. Toussaint O, Royer V, Salmon M, Remacle J. Stress-induced premature senescence and tissue ageing. Biochem Pharmacol. 2002;64(5-6):1007-9.

6. Campisi J. Cellular senescence as tumor-suppressor mechanism. Trends Cell Biol. 2001; 11:27–31.

7. Campisi J. Senescent cells, tumor suppression and organismal aging. Good citizens, bad neighbors. Cell. 2005; 120:513–522.

8. Murphy C. T., McCarroll S. A., Bargmann C. I., Fraser A., Kamath R. S., Ahringer J., Li H., Kenyon C. 2003Genes that act downstream of DAF-16 to influence the lifespan of Caenorhabditis elegans. Nature 424, 277–284 (doi:10.1038/nature01789) 10.1038/nature017894.

9. Kirkwood T. B. L. 2005 Understanding the odd science of ageing. Cell 120, 437–447 (doi: 10.1016/j.cell.2005.01.027) 10.1016/j.cell.2005.01.027

10. Kirkwood, Thomas B. L. “Systems Biology of Ageing and Longevity.” *Philosophical Transactions of the Royal Society B: Biological Sciences*366.1561 (2011): 64–70. *PMC*.

11. Koschmann, Jeannette, Anirban Bhar, Philip Stegmaier, Alexander Kel, and Edgar Wingender. "“Upstream Analysis”: An Integrated Promoter-Pathway Analysis Approach to Causal Interpretation of Microarray Data." Microarrays 4.2 (2015): 270-86.

12. Pazolli E, Luo X, Brehm S, Carbery K et al. Senescent stromal-derived osteopontin promotes preneoplastic cell growth. Cancer Res 2009;69(3):1230-9.

13. Wettenhall JM, Smyth GK. limmaGUI: a graphical user interface for linear modeling of microarray data. Bioinformatics. 2004;20(18):3705-6.

14. Computational Biology Solutions using R and Bioconductor. R. Gentleman, V. Carey, S. Dudoit, R. Irizarry, W. Huber (eds), Springer, New York, 2005.

15. Krull M, Pistor S, Voss N, Kel A, Reuter I, Kronenberg D, Michael H, Schwarzer K, Potapov A, Choi C, Kel-Margoulis O, Wingender E. TRANSPATH: an information resource for storing and visualizing signaling pathways and their pathological aberrations. Nucleic Acids Res. 2006;34(Database issue):D546-51.

16. Matys V, Kel-Margoulis OV, Fricke E, Liebich I, Land S, Barre-Dirrie A, Reuter I, Chekmenev D, Krull M, Hornischer K, Voss N, Stegmaier P, Lewicki-Potapov B, Saxel H, Kel AE, Wingender E. TRANSFAC and its module TRANSCompel: transcriptional gene regulation in eukaryotes. Nucleic Acids Res. 2006;34(Database issue):D108-10.

17. Kel A, Voss N, Jauregui R, Kel-Margoulis O, Wingender E. Beyond microarrays: find key transcription factors controlling signal transduction pathways. BMC Bioinformatics. 2006; 7 Suppl 2:S13.

18. Kel AE, Gössling E, Reuter I, Cheremushkin E, Kel-Margoulis OV, Wingender E. MATCH: A tool for searching transcription factor binding sites in DNA sequences. Nucleic Acids Res. 2003; 31(13):3576-9.

19. Stepanova M, Tiazhelova T, Skoblov M, Baranova A. A comparative analysis of relative occurrence of transcription factor binding sites in vertebrate genomes and gene promoter areas. Bioinformatics. 2005; 21(9):1789-96.

20. Cahan P, Rovegno F, Mooney D, Newman JC, St Laurent G 3rd, McCaffrey TA. Meta-analysis of microarray results: challenges, opportunities, and recommendations for standardization. Gene. 2007; 401(1-2):12-8

21. Yang IS, Kim S. Analysis of Whole Transcriptome Sequencing Data: Workflow and Software. Genomics Inform. 2015; 13(4):119-25.

22. Piwowar HA, Day RS, Fridsma DB. Sharing detailed research data is associated with increased citation rate. PLoS One. 2007; 2(3):e308.

23. Yilmaz Y. Systematic review: caspase-cleaved fragments of cytokeratin 18 – the promises and challenges of a biomarker for chronic liver disease. Aliment Pharmacol Ther. 2009 Dec 1;30(11-12):1103-9.

24. Shagisultanova E, Dunbrack RL Jr, Golemis EA. Issues in interpreting the in vivo activity of Aurora-A. Expert Opin Ther Targets. 2015 Feb;19(2):187-200.

25. Geigl JB, Langer S, Barwisch S, Pfleghaar K, Lederer G, Speicher MR. Analysis of gene expression patterns and chromosomal changes associated with aging. Cancer Res. 2004 Dec 1;64(23):8550-7.

26. Dekker P, Gunn D, McBryan T, Dirks RW, van Heemst D, Lim FL, Jochemsen AG, Verlaan-de Vries M, Nagel J, Adams PD, Tanke HJ, Westendorp RG, Maier AB.

Microarray-based identification of age-dependent differences in gene expression of human dermal fibroblasts. Mech Ageing Dev. 2012 Jul;133(7):498-507.

27. Begley L, Monteleon C, Shah RB, Macdonald JW, Macoska JA. CXCL12 overexpression and secretion by aging fibroblasts enhance human prostate epithelial proliferation in vitro. Aging Cell. 2005 Dec;4(6):291-8.

28. Hoffmeyer K, Raggioli A, Rudloff S, Anton R, Hierholzer A, Del Valle I, Hein K, Vogt R, Kemler R. Wnt/β-catenin signaling regulates telomerase in stem cells and cancer cells. Science. 2012 Jun 22;336(6088):1549-54.

29. Harten IA, Zahr RS, Lemire JM, Machan JT, Moses MA, Doiron RJ, Curatolo AS, Rothman FG, Wight TN, Toole BP, Gordon LB. Age-dependent loss of MMP-3 in Hutchinson-Gilford progeria syndrome. J Gerontol A Biol Sci Med Sci. 2011 Nov;66(11):1201-7.

30. Vierkötter A, Schikowski T, Sugiri D, Matsui MS, Krämer U, Krutmann J. MMP-1 and -3 promoter variants are indicative of a common susceptibility for skin and lung aging: results from a cohort of elderly women (SALIA). J Invest Dermatol. 2015 May;135(5):1268-74.

31. Stallings-Mann ML, Waldmann J, Zhang Y, Miller E, Gauthier ML, Visscher DW, Downey GP, Radisky ES, Fields AP, Radisky DC. Matrix metalloproteinase induction of Rac1b, a key effector of lung cancer progression. Sci Transl Med. 2012 Jul 11;4(142):142ra95.

32. Mehner C, Miller E, Khauv D, Nassar A, Oberg AL, Bamlet WR, Zhang L, Waldmann J, Radisky ES, Crawford HC, Radisky DC. Tumor cell-derived MMP3 orchestrates Rac1b and tissue alterations that promote pancreatic adenocarcinoma. Mol Cancer Res. 2014 Oct;12(10):1430-9.

33. Ding N, Nie H, Sun X, Sun W, Qu Y, Liu X, Yao Y, Liang X, Chen CC, Li Y. Human serum N-glycan profiles are age and sex dependent. Age Ageing. 2011 Sep;40(5):568-75.

34. Vanhooren V, Dewaele S, Libert C, Engelborghs S, De Deyn PP, Toussaint O, Debacq-Chainiaux F, Poulain M, Glupczynski Y, Franceschi C, Jaspers K, van der Pluijm I, Hoeijmakers J, Chen CC. Serum N-glycan profile shift during human ageing. Exp Gerontol. 2010 Oct;45(10):738-43.

35. Semren N, Welk V, Korfei M, Keller IE, Fernandez IE, Adler H, Günther A, Eickelberg O, Meiners S. Regulation of 26S Proteasome Activity in Pulmonary Fibrosis. Am J Respir Crit Care Med. 2015 Nov 1;192(9):1089-101.

36. Venkataraman K, Futerman AH. Do longevity assurance genes containing Hox domains regulate cell development via ceramide synthesis? FEBS Lett. 2002 Sep 25;528(1-3):3-4.

37. Tacutu R, Craig T, Budovsky A, Wuttke D, Lehmann G, Taranukha D, Costa J, Fraifeld VE, de Magalhães JP. Human Ageing Genomic Resources: integrated databases and tools for the biology and genetics of ageing. Nucleic Acids Res. 2013 Jan;41(Database issue):D1027-33.

38. Sfikas A, Batsi C, Tselikou E, Vartholomatos G, Monokrousos N, Pappas P, Christoforidis S, Tzavaras T, Kanavaros P, Gorgoulis VG, Marcu KB, Kolettas E. The canonical NF-κB pathway differentially protects normal and human tumor cells from ROS-induced DNA damage. Cell Signal. 2012 Nov;24(11):2007-23.

39. Liu C, La Rosa S, Hagos EG. Oxidative DNA damage causes premature senescence in mouse embryonic fibroblasts deficient for Krüppel-like factor 4. Mol Carcinog. 2015 Sep;54(9):889-99.

40. Zhang W, Ji W, Yang L, Yao L, Wang G, Xuan A, Zhuang Z. The involvement of epigenetic silencing of Foxa2 in cellular replicative and premature senescence induced by hydrogen peroxide. Free Radic Res. 2013 Apr;47(4):325-32.

41. Sadaie M, Dillon C, Narita M, Young AR, Cairney CJ, Godwin LS, Torrance CJ, Bennett DC, Keith WN, Narita M. Cell-based screen for altered nuclear phenotypes reveals senescence progression in polyploid cells after Aurora kinase B inhibition. Mol Biol Cell. 2015 Sep 1;26(17):2971-85.

42. McEvilly RJ, Erkman L, Luo L, Sawchenko PE, Ryan AF, Rosenfeld MG. Requirement for Brn-3.0 in differentiation and survival of sensory and motor neurons. Nature. 1996 Dec 12;384(6609):574-7.

43. Hohenauer T, Berking C, Schmidt A, Haferkamp S, Senft D, Kammerbauer C, Fraschka S, Graf SA, Irmler M, Beckers J, Flaig M, Aigner A, Höbel S, Hoffmann F, Hermeking H, Rothenfusser S, Endres S, Ruzicka T, Besch R. The neural crest transcription factor Brn3a is expressed in melanoma and required for cell cycle progression and survival. EMBO Mol Med. 2013 Jun;5(6):919-34.

44. Liu T, Zhou W, Cai B, Chu J, Shi G, Teng H, Xu J, Xiao J, Wang Y. IRX2-mediated upregulation of MMP-9 and VEGF in a PI3K/AKT-dependent manner. Mol Med Rep. 2015 Sep;12(3):4346-51.

45. Liu T, Zhou W, Zhang F, Shi G, Teng H, Xiao J, Wang Y. Knockdown of IRX2 inhibits osteosarcoma cell proliferation and invasion by the AKT/MMP9 signaling pathway. Mol Med Rep. 2014 Jul;10(1):169-74.

46. Kowalik L, Hudspeth AJ. A search for factors specifying tonotopy implicates DNER in hair-cell development in the chick's cochlea. Dev Biol. 2011 Jun 15;354(2):221-31.

47. Faryna M, Konermann C, Aulmann S, Bermejo JL, Brugger M, Diederichs S, Rom J, Weichenhan D, Claus R, Rehli M, Schirmacher P, Sinn HP, Plass C, Gerhauser C. Genome-wide methylation screen in low-grade breast cancer identifies

novel epigenetically altered genes as potential biomarkers for tumor diagnosis. FASEB J. 2012 Dec;26(12):4937-50.

48. Kitchen MO, Bryan RT, Emes RD, Glossop JR, Luscombe C, Cheng KK, Zeegers MP, James ND, Devall AJ, Mein CA, Gommersall L, Fryer AA, Farrell WE. Quantitative genome-wide methylation analysis of high-grade non-muscle invasive bladder cancer. Epigenetics. 2016 Mar 3;11(3):237-46.

49. Delgado-Calle J, Fernández AF, Sainz J, Zarrabeitia MT, Sañudo C, García-Renedo R, Pérez-Núñez MI, García-Ibarbia C, Fraga MF, Riancho JA. Genome-wide profiling of bone reveals differentially methylated regions in osteoporosis and osteoarthritis. Arthritis Rheum. 2013 Jan;65(1):197-205.

50. Gravallese EM. Osteopontin: a bridge between bone and the immune system. J Clin Invest. 2003 Jul;112(2):147-9.

51. Jiang SS, Chen CH, Tseng KY, Tsai FY, Wang MJ, Chang IS, Lin JL, Lin S. Gene expression profiling suggests a pathological role of human bone marrow-derived mesenchymal stem cells in aging-related skeletal diseases. Aging (Albany NY). 2011 Jul;3(7):672-84.

52. Hsu YH, Zillikens MC, Wilson SG, Farber CR, Demissie S, Soranzo N, Bianchi EN, Grundberg E, Liang L, Richards JB, Estrada K, Zhou Y, van Nas A, Moffatt MF, Zhai G, Hofman A, van Meurs JB, Pols HA, Price RI, Nilsson O, Pastinen T, Cupples LA, Lusis AJ, Schadt EE, Ferrari S, Uitterlinden AG, Rivadeneira F, Spector TD, Karasik D, Kiel DP. An integration of genome-wide association study and gene expression profiling to prioritize the discovery of novel susceptibility loci for osteoporosis-related traits. PLoS Genet. 2010 Jun 10;6(6):e1000977.

53. Pazolli E, Alspach E, Milczarek A, Prior J, Piwnica-Worms D, Stewart SA. Chromatin remodeling underlies the senescence-associated secretory phenotype of tumor stromal fibroblasts that supports cancer progression. Cancer Res. 2012 May 1;72(9):2251-61.

BIOGRAPHY

Kamil Can Kural graduated from Maltepe Anatolian High school, Istanbul, Turkey, at 2010. He received his Bachelor of Science in Biological and Chemical Engineering from Istanbul Technical University and Montana State University Dual Degree Program at 2014. He received his Master of Science in Computational Biology and Bioinformatics from George Mason University at 2016.